TECHNICAL REPORT BRL-TR-3213

BRL

CALCULATIONS OF THRUST GENERATION BY THE DRIVER SYSTEM OF A LARGE BLAST SIMULATOR

STEPHEN J. SCHRAML

MARCH 1991

U.S. ARMY LABORATORY COMMAND

BALLISTIC RESEARCH LABORATORY
ABERDEEN PROVING GROUND, MARYLAND

NOTICES

Destroy this report when it is no longer needed. DO NOT return it to the originator.

Additional copies of this report may be obtained from the National Technical Information Service, U.S. Department of Commerce, 5285 Port Royal Road, Springfield, VA 22161.

The findings of this report are not to be construed as an official Department of the Army position, unless so designated by other authorized documents.

The use of trade names or manufacturers' names in this report does not constitute indorsement of any commercial product.

REPORT DOCUMENTATION PAGE

Form Approved
OMB No. 0704-0188

1. AGENCY USE ONLY (Leave blank)	2. REPORT DATE	3. REPORT TYPE AND DATES COVERED
	March 1991	Final, Feb 90 - Dec 90

4. TITLE AND SUBTITLE

Calculations of Thrust Generation by the Driver System of a Large Blast Simulator

5. FUNDING NUMBERS

1L162120AH25

6. AUTHOR(S)

Stephen J. Schraml

7. PERFORMING ORGANIZATION NAME(S) AND ADDRESS(ES)

Director
U.S. Army Ballistic Research Laboratory
ATTN: SLCBR-TB-B
Aberdeen Proving Ground, MD 21005-5066

8. PERFORMING ORGANIZATION REPORT NUMBER

9. SPONSORING/MONITORING AGENCY NAME(S) AND ADDRESS(ES)

U.S. Army Ballistic Research Laboratory
ATTN: SLCBR-DD-T
Aberdeen Proving Ground, MD 21005-5066

10. SPONSORING/MONITORING AGENCY REPORT NUMBER

BRL-TR-3213

11. SUPPLEMENTARY NOTES

This work was performed under the auspices of the U.S. Army Harry Diamond Laboratories, ATTN: SLCHD-NW-P, 2800 Powder Mill Road, Adelphi, MD 20783-1197

12a. DISTRIBUTION/AVAILABILITY STATEMENT

Approved For Public Release; Distribution Unlimited.

12b. DISTRIBUTION CODE

13. ABSTRACT *(Maximum 200 words)*

A computational study was performed to determine the peak thrust which would be generated by cylindrical shock tube drivers of various lengths. Thrust histories were generated for two different flow conditions, one in which the shock tube was operated normally and the other in which a driver length adjusting device (hydroplug) failed.

Once the magnitude and behavior of the thrust histories are understood, steps can be taken to design supports for the driver tubes which will withstand the cyclic loading associated with normal operation as well as the reverse loading associated with the component failure.

14. SUBJECT TERMS

Blast; Blast Tubes; Flow Fields; Gas Dynamics; Nuclear Explosion Simulation; Nuclear Weapons; Shock Tubes; Shock Waves; Thrust

15. NUMBER OF PAGES

57

16. PRICE CODE

17. SECURITY CLASSIFICATION OF REPORT	18. SECURITY CLASSIFICATION OF THIS PAGE	19. SECURITY CLASSIFICATION OF ABSTRACT	20. LIMITATION OF ABSTRACT
UNCLASSIFIED	UNCLASSIFIED	UNCLASSIFIED	UNLIMITED

INTENTIONALLY LEFT BLANK.

Table of Contents

INTENTIONALLY LEFT BLANK.

List of Figures

List of Figures (Continued)

I. Background

The U.S. Army Ballistic Research Laboratory (BRL) has been conducting research to support the design of a facility intended to subject full scale military equipment to the blast and thermal environment produced by tactical nuclear weapons. The design of this facility, termed the Large Blast/Thermal Simulator (LB/TS) [1], is being directed by the Army Corps of Engineers through the Defense Nuclear Agency. An illustration of the proposed LB/TS can be seen in Figure 1.

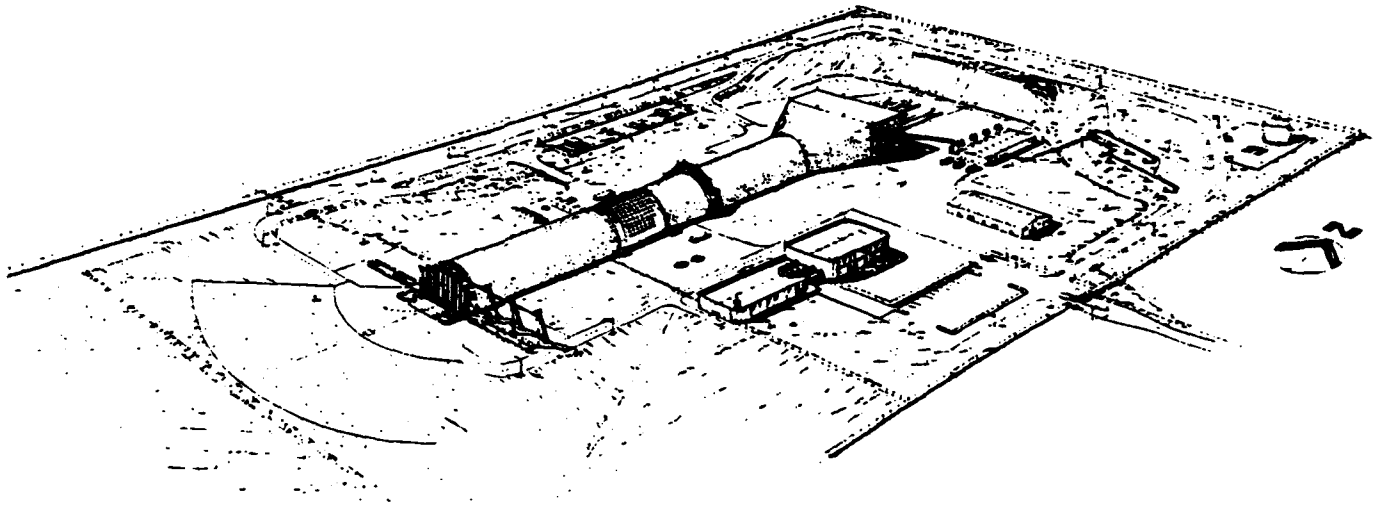

Figure 1. The Proposed Large Blast/Thermal Simulator

As currently conceived the LB/TS, when completed, will be the world's largest shock tube. A shock tube is a device in which compressed gas is quickly released from a reservoir to form a shock wave which travels down its expansion section. By adjusting the volume of the gas reservoir (also known as the driver) and the initial reservoir pressure and temperature, a nuclear blast wave of desired shock overpressure and weapon yield can be simulated. The LB/TS is designed so that a wide range of nuclear blast waves can be simulated. Shock overpressures in the simulator can range from $2 - 35$ *psi* and simulated weapon yield can range from $1 - 600$ kT.

Conventional shock tubes usually have a single driver. The LB/TS will have a total of nine separate driver tubes. The downstream end of each driver tube has a converging nozzle and a cylindrical throat section. Located in each throat is a pair of diaphragms. The flow in the LB/TS is initiated through the simultaneous rupturing of the diaphragms in the nine

drivers. Some of the driver tubes, with their respective nozzles and diaphragms, can be seen in Figure 2, which is a schematic diagram of the LB/TS.

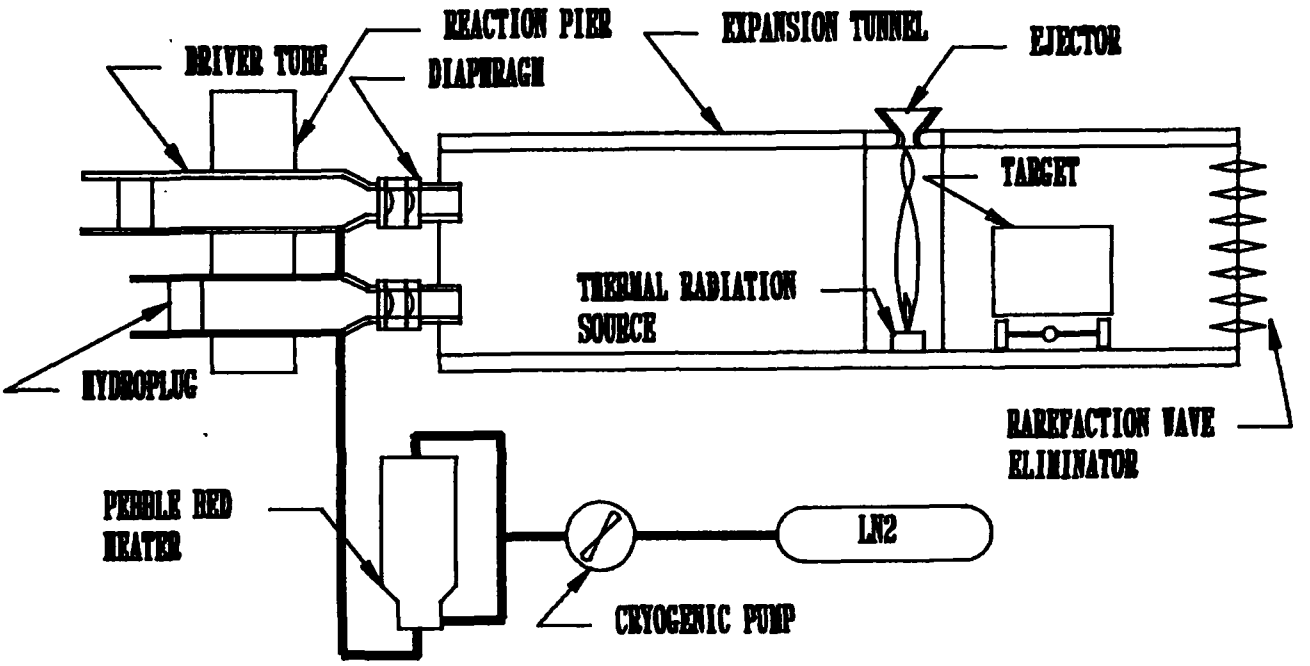

Figure 2. Schematic Diagram of the Large Blast/Thermal Simulator

When the diaphragms are ruptured and the gas rushes out of the driver tubes, thrust is generated which applies a force to each driver tube. The applied force acts in the opposite direction of the flow. In order to design a restraint system capable of counteracting these forces, the maximum expected thrust history for each driver tube must be determined. This report documents efforts by the Ballistic Research Laboratory to estimate the thrust history for each driver tube when charged with its maximum operating pressure. In all the calculations performed for this study, the initial driver pressure and temperature were 15.615 *MPa* and 650 K, respectively, while the ambient pressure and temperature used were 101.325 *kPa* and 288.15 K.

As previously stated, the volume of the driver tubes can be adjusted to simulate a wide range of blast waves. As the volume of the driver tubes is decreased, the simulated weapon yield for a particular set of driver conditions decreases. The volume of a driver tube is adjusted by positioning a device known as a hydroplug in the tube. A hydroplug, shown in Figure 2, is a large cylindrical device that roughly resembles a bank vault door. It is made primarily of steel and is equipped with metallic wedges which are expanded against the driver tube walls to hold the hydroplug in place. When a hydroplug is locked in position, its elastomeric rings provide a seal between itself and the wall of the driver, preventing high pressure driver gas from escaping around its perimeter. One scenario which is of concern to the design of the LB/TS is that in which a hydroplug should become dislodged after the

driver tubes have been pressurized. If this were to happen, thrust would be generated on the driver tube which would try to force it into the expansion section of the LB/TS. This thrust acts in the opposite direction of the case in which the LB/TS is operated normally. So that the loads associated with this type of scenario may be incorporated into the design of the LB/TS, an effort was taken to estimate the thrust histories in the event that a hydroplug should fail.

The calculations described in this report were performed using Version 122 of the HULL hydrocode [2]. All calculations employed two-dimensional grids with axial symmetry. The HULL code is an inviscid code. Therefore, forces on the driver walls resulting from fluid friction were not considered. All thrust histories were calculated by summing the hydrostatic pressure on the surfaces of the driver tubes for a given point in time.

The gridding scheme in the HULL code uses rectangular cells. The accuracy at which lines that do not run horizontally or vertically are modeled is a function of the width and height of the cells. If the grid has very small cells, then a diagonal line, for instance, will be modeled with greater accuracy than it would with larger cells. The same is true for curved surfaces. However, the price one pays for small cells is large. In a two-dimensional explicit time-stepping hydrocode, the change in run time caused by a change in cell size is proportional to the cube of the ratio of the old and new cell widths. For example, a calculation with square cells 1 *cm* wide will consume eight times as much processor time as an equivalent 2 *cm* cell run. With this in mind, an acceptable combination of model accuracy and computational economy was chosen for the calculations discussed in this report.

II. Driver Tube Layout in the LB/TS

There are a total of nine driver tubes in the current design of the LB/TS. Four different driver lengths are divided among these nine drivers [3]. Two driver tubes are 14.000 *m* long, three are 18.666 *m*, two are 27.200 *m* and two are 36.159 *m* long. All the driver tubes are equipped with hydroplugs except for the two 14.000 *m* tubes which have hemispherical heads at their upstream ends. The lengths listed here represent only the cylindrical driver tube from the downstream end of the hydroplug to the beginning of the converging nozzle for those drivers with hydroplugs. In the case of the two 14.000 *m* drivers, the length is defined by the distance from the radial center of the hemispherical head to the beginning of the converging nozzle.

The expansion section of the LB/TS is semicircular. The driver tubes are arranged so that the flow from the drivers will fill the expansion section as evenly as possible. Any two driver tubes of equal length are located on opposite sides of the expansion section, equidistant from the centerline of the expansion section. The set of three 18.666 *m* tubes has one of its tubes on each side of the expansion section with the third tube in the center of the expansion section. With this arrangement, no torsional moments are applied to the driver tube reaction pier during normal operation. The arrangement and numbering of the driver tubes is illustrated in Figure 3.

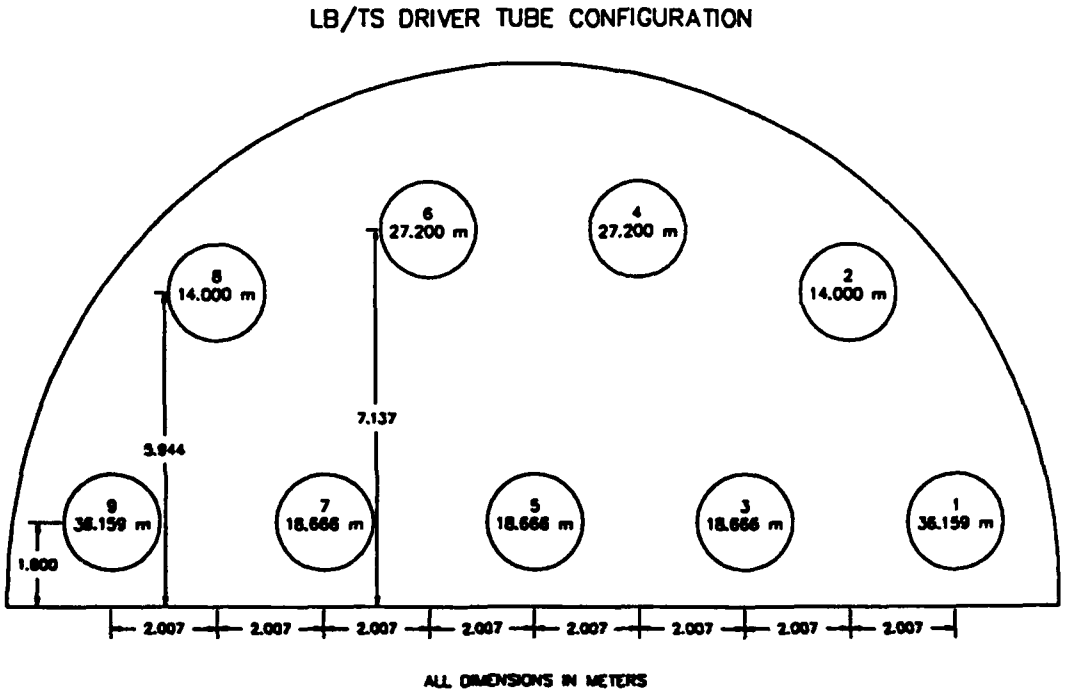

Figure 3. Location of Driver Tubes in the LB/TS, Facing the Drivers from a Position Inside the Expansion Section

III. Normal Operation

Because there are only four unique driver tube lengths, only four thrust histories need to be determined. In an effort to keep the calculations as simple and economical as possible, only one driver tube was modeled in any one run. The computational model of one of the driver tubes can be seen in Figure 4.

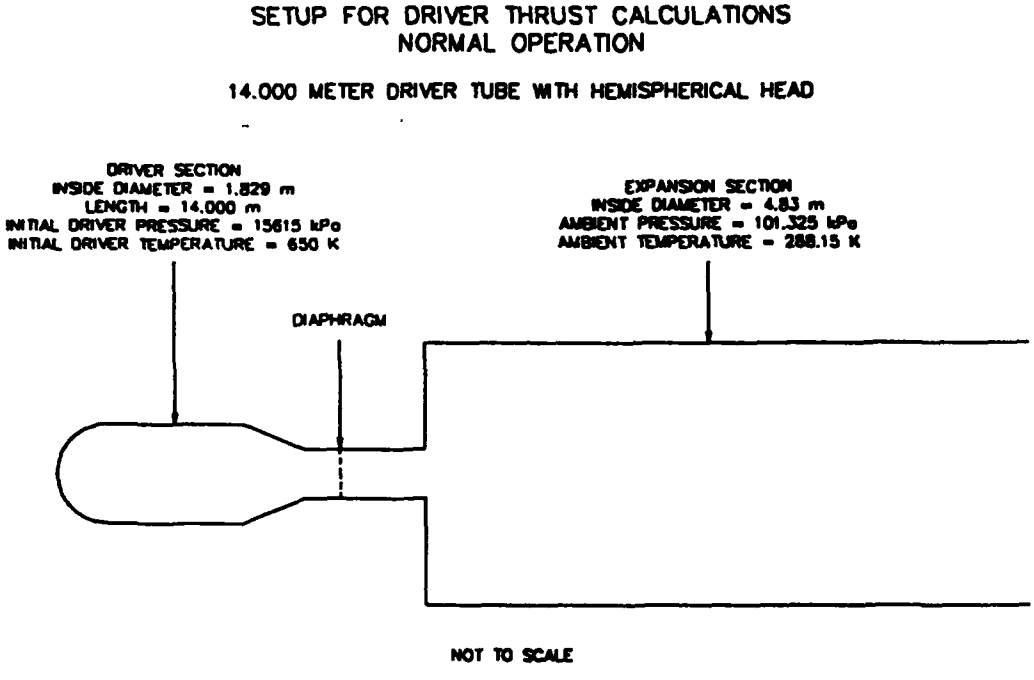

Figure 4. Computational Model for Normal Operation Calculations

The ratio of the area of the expansion section to the combined area of the nine throat sections is 28:1. If it is assumed that the flow from each driver tube equally fills one ninth of the expansion section, then the area ratio seen by the flow in going from one throat into the expansion section will be 28:1. Since only one driver tube would be modeled at a time, the area of the expansion section in the calculations is set at 28 times the area of one throat section. Also, in the computational model, the expansion section was made very long so that disturbances generated when the shock reached the downstream boundary would not effect the flow in the driver during the computation.

The resulting thrust histories can be seen in Figures 5 through 8. For the most part, one can see that the amplitude of the pressure waves is about the same for each of the four thrust histories. The timing of the passing of the waves in the drivers is the cause of the differences between the histories.

Each of the thrust histories starts at time equal to zero with an initial thrust of about 10.19 million Newtons. When the flow is initiated, the gas begins to travel in the downstream

direction. At the same time, a rarefaction wave begins to move in the upstream direction into the driver. As this rarefaction wave passes over the converging nozzle, the pressure on the surface of the converging nozzle decreases, resulting in an increase in net thrust. This is illustrated by the first peak in the thrust histories at about 16 million Newtons. This peak is held roughly constant until the rarefaction wave meets the upstream end of the driver tube. When this occurs, the pressure on the upstream wall of the tube drops resulting in a substantial drop in thrust. After the rarefaction wave meets the upstream end of the tube it is reflected and begins to travel downstream where it is eventually reflected again at the throat and the process starts over again. It is this repeated motion of the rarefaction wave in the driver which gives the thrust history its cyclic pattern. Each passage of this rarefaction wave causes the pressure in the driver to drop. This decrease in driver pressure causes the underlying decay seen in the oscillating thrust histories.

The thrust histories illustrated in Figures 5 to 8 are for single driver tubes. To obtain the total thrust from all nine driver tubes that would be seen by the reaction pier, the individual thrust histories were multiplied by the number of driver tubes for each length and then summed. The resulting total thrust history can be seen in Figure 9. As one would expect, the peak thrust is nine times the peak for one driver tube. The total thrust history differs from the individual thrust histories in that its cyclic pattern is less apparent. This is caused by the difference in frequencies between the thrust histories for driver tubes of different lengths. When summing the histories of varying frequencies, the decaying nature of the thrust history becomes more obvious.

These thrust histories are the expected result of operating the LB/TS at its maximum design limits of driver pressure, driver temperature and driver volume. Lower driver pressures would result in lower peak thrust values. A smaller driver volume would dictate a quicker decay in the thrust histories. By using these maximum expected thrust histories, the LB/TS driver support system can be designed to withstand the expected loads under normal, repeated operation.

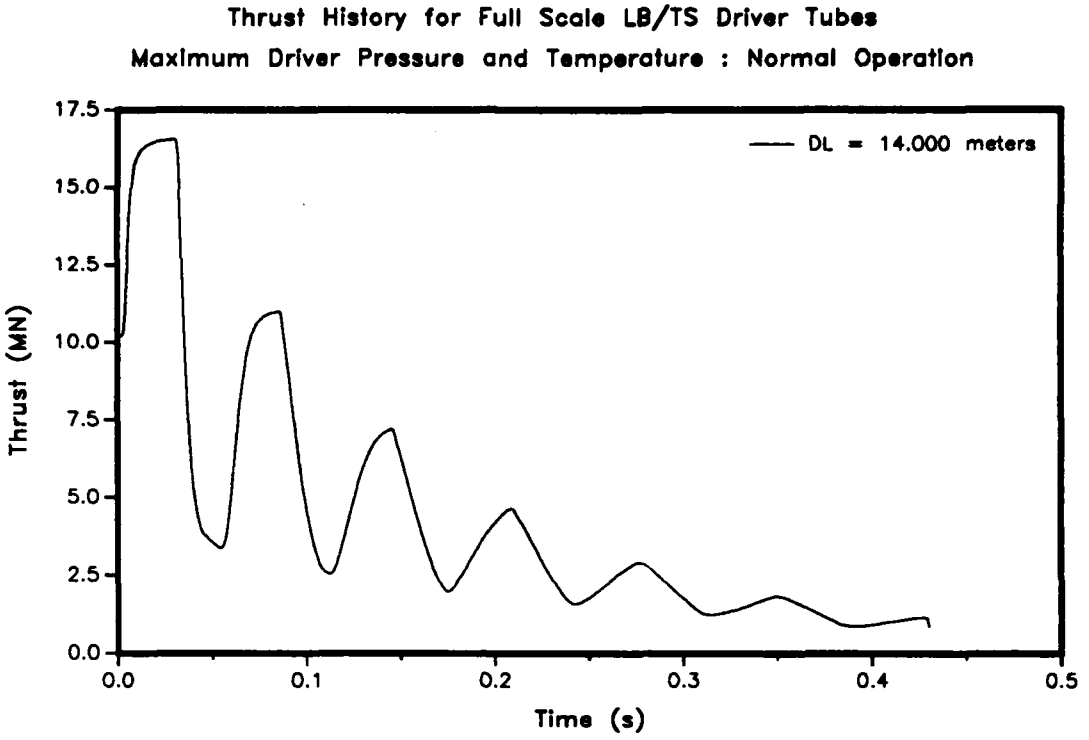

Figure 5. Thrust History for 14.000 m Driver Tube; Normal Operation

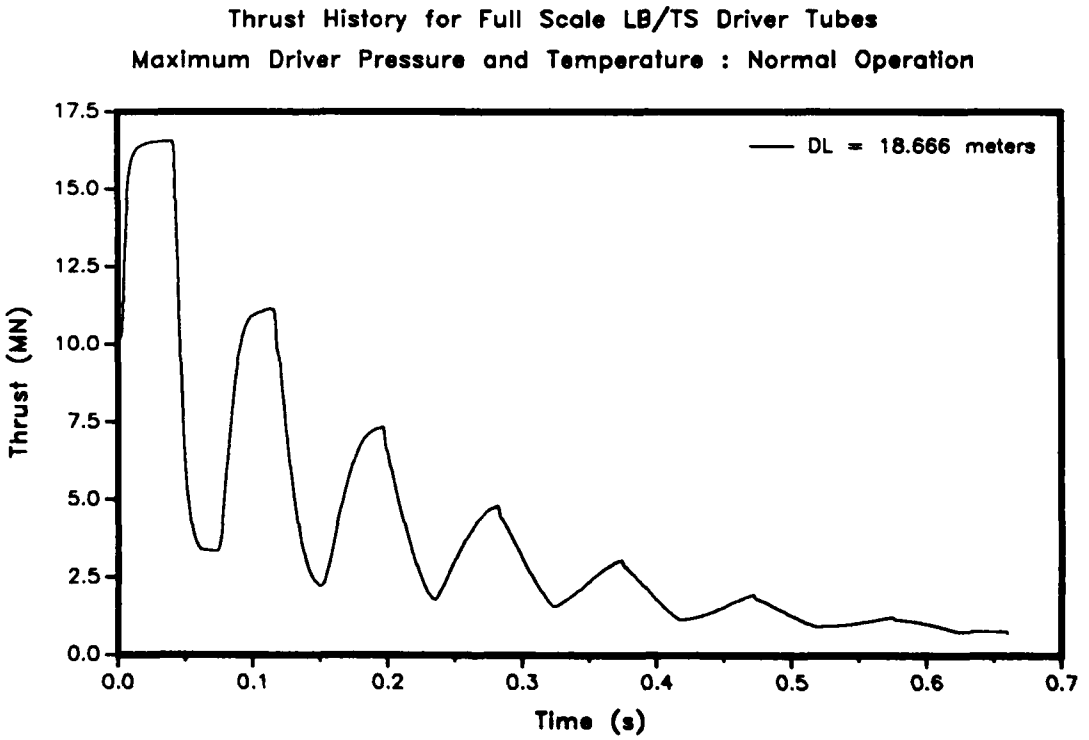

Figure 6. Thrust History for 18.666 m Driver Tube; Normal Operation

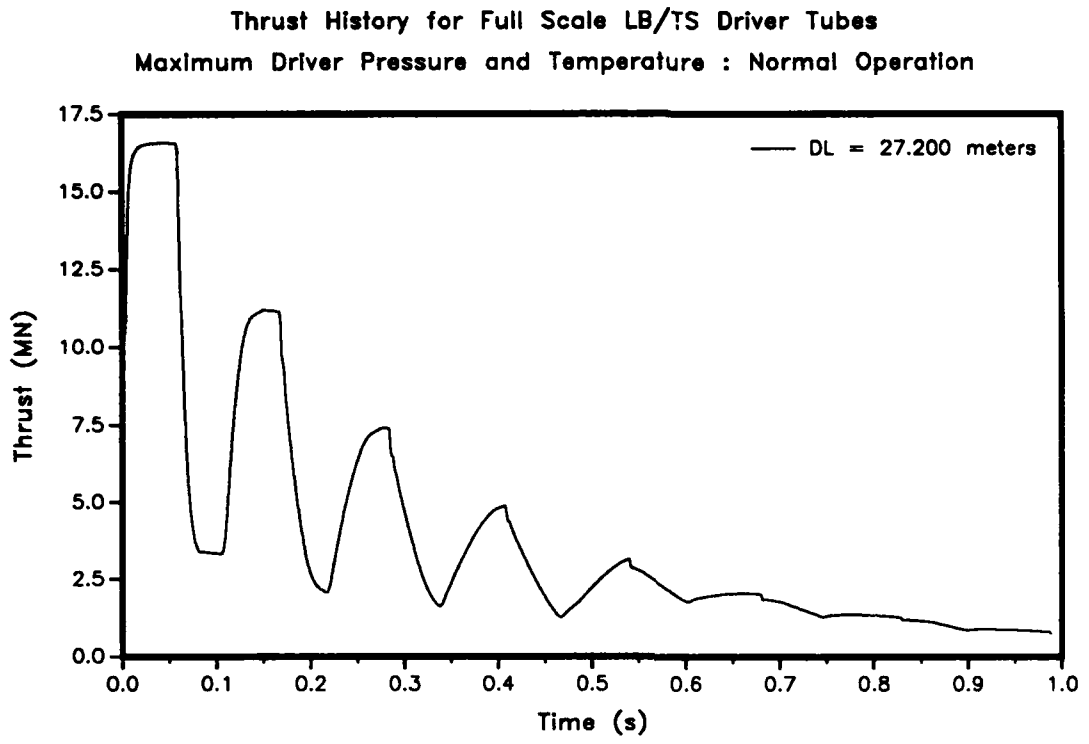

Figure 7. Thrust History for 27.200 m Driver Tube; Normal Operation

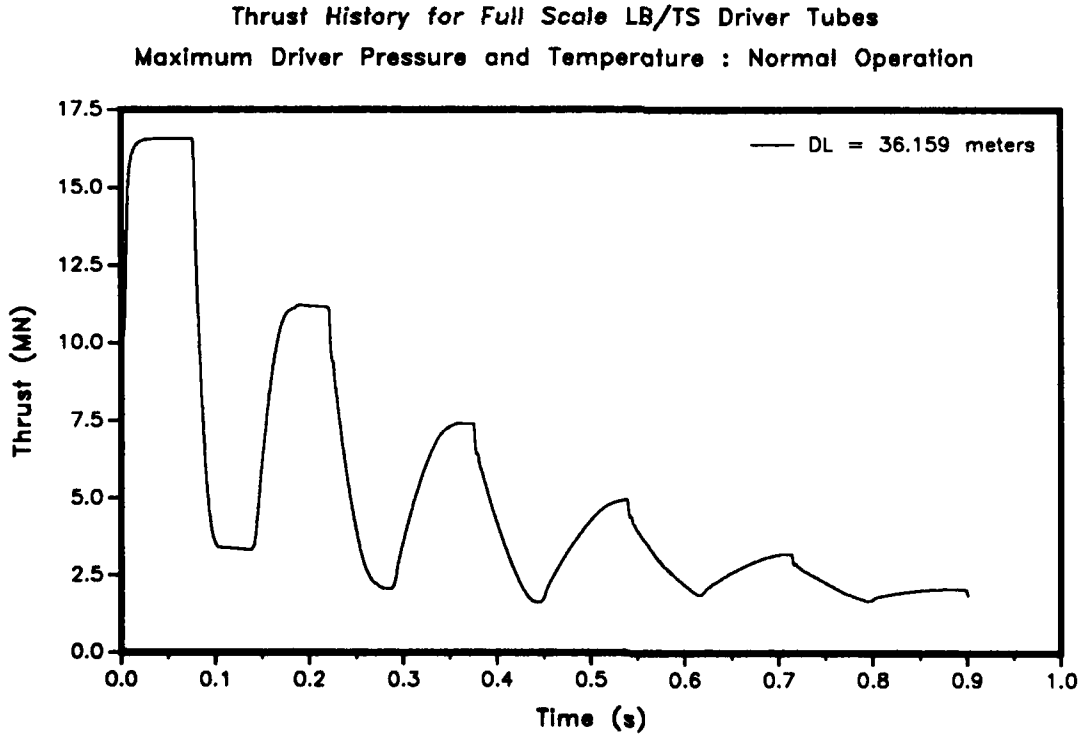

Figure 8. Thrust History for 36.159 m Driver Tube; Normal Operation

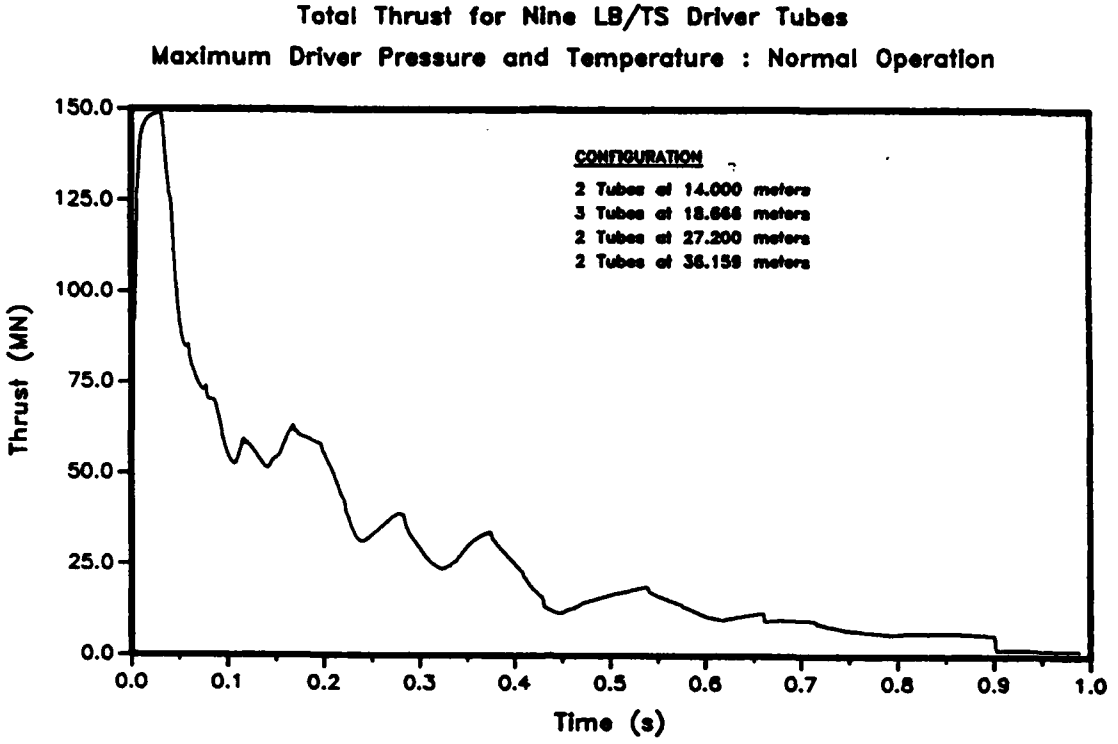

Figure 9. Total Thrust History All Driver Tubes; Normal Operation

IV. Hydroplug Failure

A hydroplug is a device which is to be used to adjust the volume in the driver tubes. Hydroplugs are currently being used in the oil industry to block a portion of pipeline while repairs or modifications are being made to the pipe. However, the hydroplugs used in the oil industry are not as large as that required for the LB/TS. Also, the temperature and pressure of the driver gas in the LB/TS will be much higher than that seen in the oil industry application. For these reasons, a decision was made to examine the thrust load which would be applied to the driver tubes in the event that a hydroplug should fail after the driver has been pressurized.

As previously stated, the HULL code was used to perform all the calculations in the study. Since HULL is a code for solving problems in hydrodynamics, it is not well suited for solving problems of multi-body dynamics. However, the multi-body dynamics codes that are available lack sufficient hydrodynamic algorithms to provide accurate aerodynamic loading data. Since the fluid forces on the driver were the desired result, the HULL code was chosen to solve the problem. Had we been interested in the interaction between the driver walls and the hydroplug, a multi-body dynamics code might have been a better choice.

The calculations of driver thrust generated from hydroplug failure were performed at the maximum expected driver temperature and pressure. For all of these calculations, the hydroplug was initially positioned at the upstream end of the driver tube. It would have

been possible to perform more calculations with the hydroplug in different initial positions, but a short schedule and the cost of computer time prohibited this.

Of the four unique driver tube lengths in the LB/TS, only the three longest will have hydroplugs. The two 14.000 m tubes will be equipped with hemispherical ends. Therefore, thrust calculations for the hydroplug failure case were only performed for the 18.666 m, 27.200 m and 36.159 m driver tubes.

Three different problem geometries were modeled to achieve the thrust histories for each of the three different driver tube lengths. The three problem geometries differed in the way the hydroplug was modeled. As the accuracy of the hydroplug model improved, the level of complexity of the calculation increased. The results of these three geometries will now be discussed in detail.

1. Simple Discontinuity

As a first order solution to the thrust calculation problem, the hydroplug itself was not modeled. Rather, the driver gas and ambient air were initially in contact with each other at a temperature/pressure discontinuity. In this setup, which can be seen in Figure 10, no attempt was made to model the dynamics of the interaction between the fluids and the hydroplug.

The resulting thrust histories for these three calculations can be seen in Figure 11. In these calculations, the thrust is initially constant at about 40.75 million Newtons. This thrust value is simply the net horizontal force on the driver determined by multiplying the initial driver overpressure by the inside diameter of the driver tube.

As in the normal operation case, the pressure discontinuity causes the flow to travel out of the driver tube in the direction of the lower pressure. At the same time, a rarefaction wave is generated and travels in the opposite direction into the driver tube. When the rarefaction wave meets the nozzle end of the driver, the pressure decreases and thus the thrust decreases. The rarefaction wave is then reflected at the diaphragm and travels back toward the position of the original discontinuity. As this reflected wave passes over the nozzle, the pressure on the nozzle is again reduced and therefore the thrust is decreased further. Since no hydroplug was modeled in these calculations, no repeated passage of waves is seen in the thrust histories. The entire driver pressure is relieved with one passage of the initial rarefaction wave.

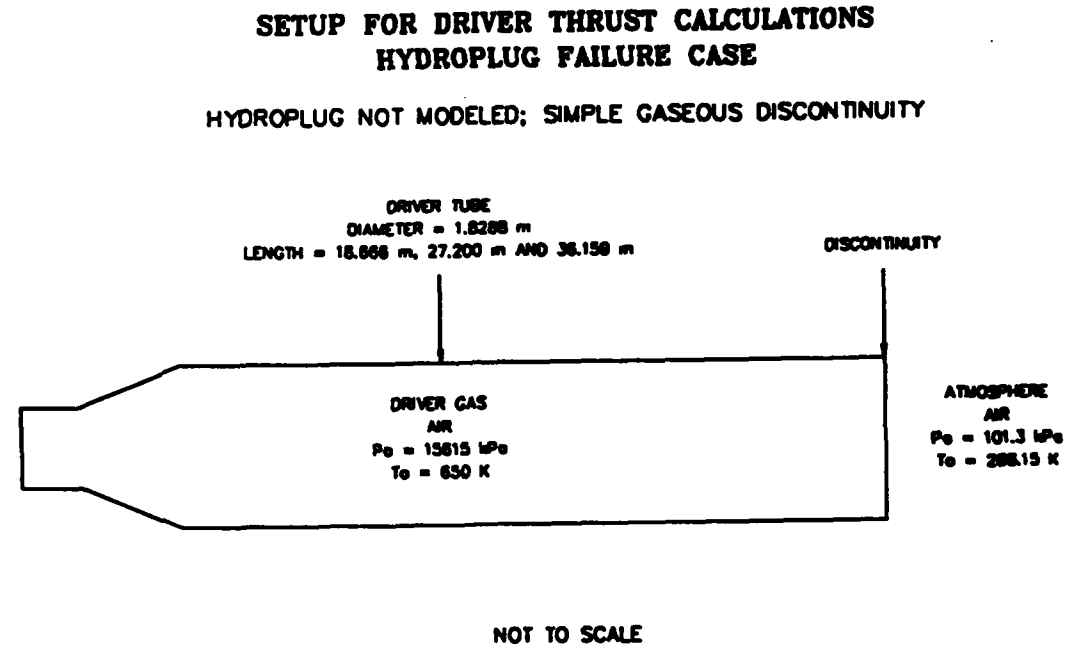

Figure 10. Computational Model for Simple Discontinuity Setup

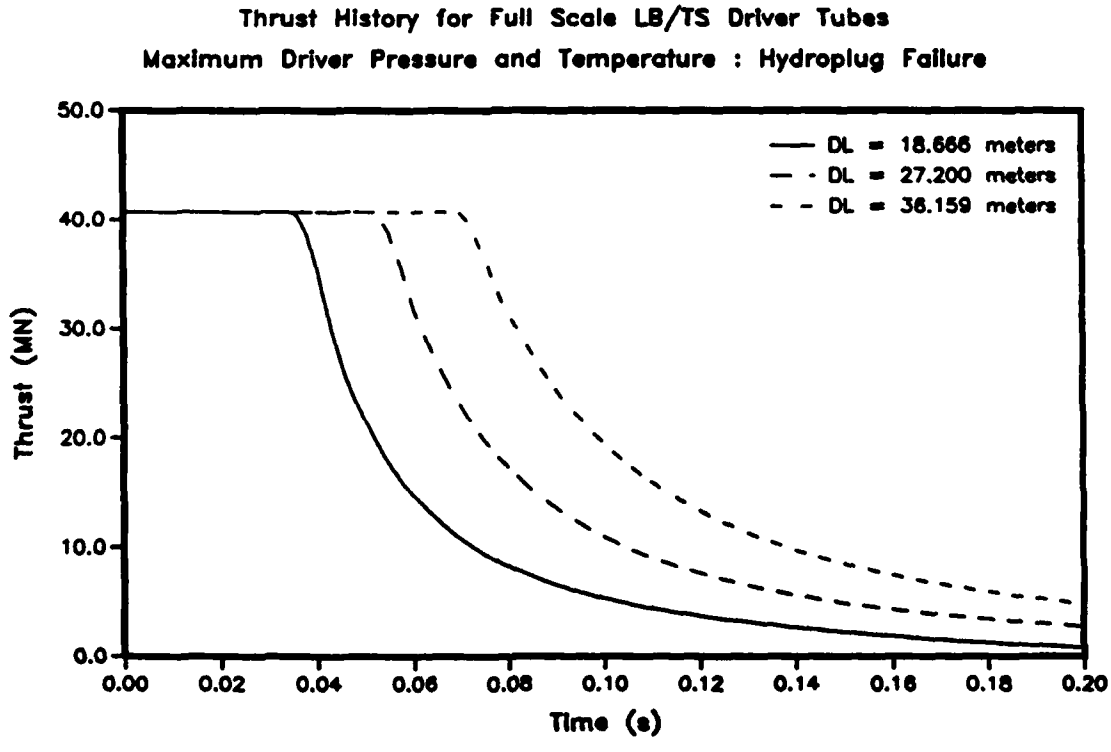

Figure 11. Thrust Histories for Simple Discontinuity Setup

2. Dense Air Mass

The hydroplug failure calculations using a simple discontinuity which were discussed previously were performed as a first order estimate. These calculations were not difficult to perform and ran in a reasonable amount of computer time. However, it was known that the effect of the hydroplug on the flow was important. Therefore, further investigation was required.

Due to the time stepping nature of this type of code, attempts to model the hydroplug as a homogeneous solid were initially avoided. The time step in a hydrocode such as HULL is determined by the spacing of the computational grid and the speed of sound plus the particle velocity of the materials in the grid. The speed of sound in a solid material such as steel is much greater than in air, which would result in a dramatically reduced time step. Therefore, this type of calculation was considered to be too time consuming to attempt.

As a compromise, a calculation was performed in which the hydroplug was modeled as a dense air mass in the 18.666 m driver tube. The setup for this calculation is shown in Figure 12. The density of the air used to model the hydroplug was defined so that the mass of dense air was equal to the mass of a hydroplug.

It was estimated that while diffusion of the air mass would occur, the diffusion might be small enough to accurately model the presence of the hydroplug. The diffusion of the air mass was observed by plotting contours of density for the computational domain at various times during the calculation. These density contours can be seen in Appendix A. The figures in this appendix show that the air mass, which served as the model of the hydroplug, experienced a great deal of diffusion.

The thrust history for this calculation is in Figure 13. In this figure the thrust history is compared to the one obtained from the simple discontinuity case for the same 18.666 m driver. Figure 13 shows that the presence of the dense air mass had a significant effect on the thrust history. It is believed that the thrust history for the dense air mass case is a better physical representation of the event when compared to the simple discontinuity case.

Like the simple discontinuity case, the thrust history for the dense air mass setup begins at a constant value of 40.75 million Newtons. The pressure differential across the dense air mass causes it to move out of the driver, in the direction of the lower pressure. When the air mass begins to move, a rarefaction wave is generated on its upstream face which travels in the upstream direction toward the diaphragm. This rarefaction wave is very similar to that generated in the simple discontinuity case, and therefore the initial decay of the thrust history is very similar to that in the simple discontinuity case. This decay is caused by the passage of the rarefaction wave over the nozzle.

Because the presence of the hydroplug is modeled, the thrust history does not decay as rapidly as that in the simple discontinuity case. This occurs because the hydroplug does not allow the gas to immediately escape from the driver. After the initial decay caused by the first rarefaction wave, the thrust history levels out at a value of about 30 million Newtons. When the upstream face of the hydroplug exits the driver tube, the driver gas is allowed to

escape from the driver which causes another rarefaction wave to be generated. This wave travels into the driver tube and decreases the pressure on the walls of the driver resulting in a decrease in thrust. With the hydroplug now out of the way, the driver gas is allowed to escape with one passage of this secondary rarefaction wave which results in the exponential decay of the thrust history.

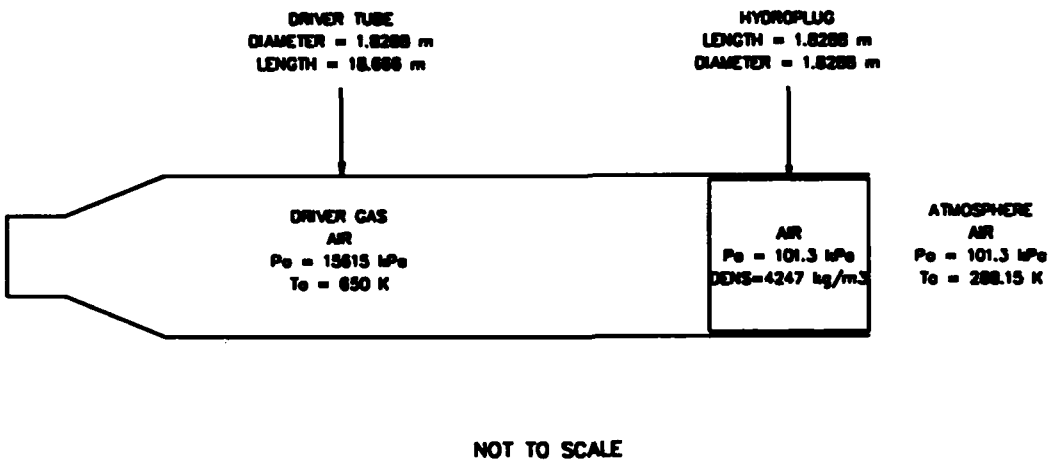

Figure 12. Computational Model for Dense Air Mass Setup

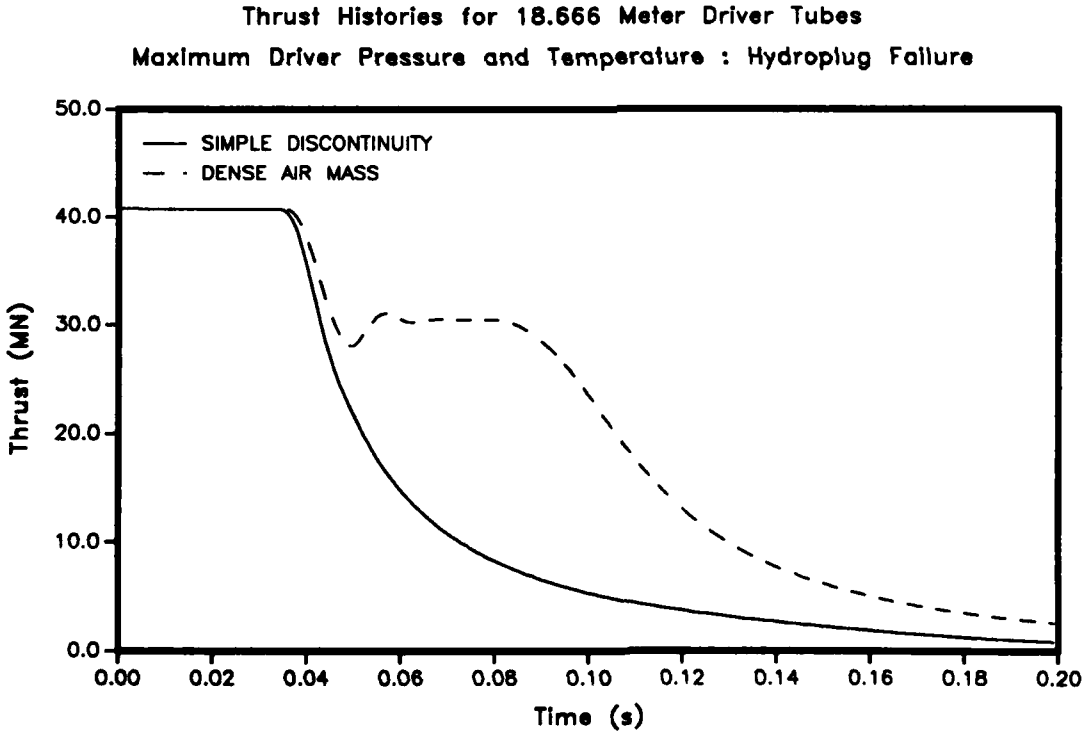

Figure 13. Thrust History for Dense Air Mass Setup

3. Steel Plug with Modified Properties

In an effort to improve the accuracy of the thrust histories for the hydroplug failure case, a final set of calculations was performed in which the hydroplug was modeled as a homogeneous steel plug with modified properties. The computational model for this calculation can be seen in Figure 14. As stated earlier, this approach was initially avoided due to the adverse effect the steel would have on the time step of the calculation. However, it was found that by altering some of the properties of the steel, the calculation could be performed without the penalty of a dramatically reduced time step.

The density of the steel in the computational model was modified so that the mass of the modeled hydroplug was equivalent to the mass of a plug proposed for the LB/TS. The time step problem was resolved by reducing the ambient sound speed in steel in the model. With these modifications, improved thrust histories could be obtained within a reasonable amount of computation time.

This practice of changing the properties of steel did not go without penalty though. The constitutive relations in this code define the sound speed in steel as the square root of the fraction of the Young's Modulus divided by the density of the homogeneous material as can be seen in Equation 1.

$$c = \sqrt{\frac{E}{\rho}} \tag{1}$$

Solving Equation 1 for Young's Modulus yields Equation 2. From Equation 2 it can be seen that by reducing the sound speed and density of steel, the Young's Modulus is significantly reduced. In the calculation, the sound speed in steel was set at 500 m/s and the density was 4247 kg/m^3. The resulting Young's Modulus, then, is 1,062 MPa which is much less than the expected value of 167,042 MPa. As a result of this reduced Young's Modulus, one would expect to see a great deal of hydroplug deformation in the calculation. This deformation, however, was considered acceptable as long as the plug remained roughly intact during the period of interest.

$$E = c^2 \rho \tag{2}$$

The value of 500 m/s for the ambient sound speed of steel was not chosen arbitrarily. So that the steel would not control the time step in the computation, a value had to be used which was less than or equal to the sound speed in the surrounding air. Using Equation 3, the initial sound speed in the driver gas was determined to be 511 m/s.

$$c = \sqrt{\gamma RT} \tag{3}$$

In Equation 3, γ is the ratio of specific heats of the ideal gas and is equal to 1.400, R is the gas constant which is 287.04 $J/kg/K$ and T is the temperature of the driver gas which is 650 K. By setting the ambient sound speed in steel at 500 m/s, the computation will

initially be controlled by the driver gas. The steel will not control the time step until late in the computation when the sound speed of the driver gas has dropped due to expansion.

As in the dense air mass case, the displacement and shape of the hydroplug were observed by plotting contours of density for the computational domain at various times during the calculation. Density contours for the 18.666 m driver tube can be seen in Appendix B. These figures illustrate that while the homogeneous steel plug did undergo some diffusion, it remained roughly intact during the period of interest. For this reason the flow of the driver gas around the plug for this calculations is considered to be more accurate than the previous two models. Therefore, the thrust histories for the calculations which used the homogeneous steel plug model are assumed to be the most accurate. These thrust histories can be seen in Figure 15.

The thrust histories in Figure 15 are very similar to the thrust history for the dense air mass case. In each, the decay of the thrust is caused by two rarefaction waves. The first wave originates at the upstream face of the hydroplug. The second wave is caused by the exiting of the hydroplug from the driver tube and subsequent acceleration of the driver gas. The primary difference between the thrust histories in the two setups is the rate of decay of the thrust caused by the first rarefaction wave.

Since the hydroplug was modeled as a compressible substance (air) in the dense air mass case, the high pressure driver gas was able to compress the hydroplug and cause it to diffuse. This resulted in a strong initial rarefaction wave.

In the case where the hydroplug was modeled as a solid steel plug with modified properties, the plug was not compressed by the driver gas and also did not experience as much diffusion as in the dense air mass case. For this reason, the initial rarefaction from the upstream face of the hydroplug did not cause as much of a decay in the thrust. The effect of the second rarefaction wave is nearly identical for the two cases.

The limited diffusion of the steel plug and the fact that the hydroplug was modeled as an incompressible medium leads us to believe that the thrust histories for this setup were the most accurate of the three cases used to model hydroplug failure. For this reason, this setup was used to generate thrust histories for each of the three driver tube lengths which are intended to receive hydroplugs.

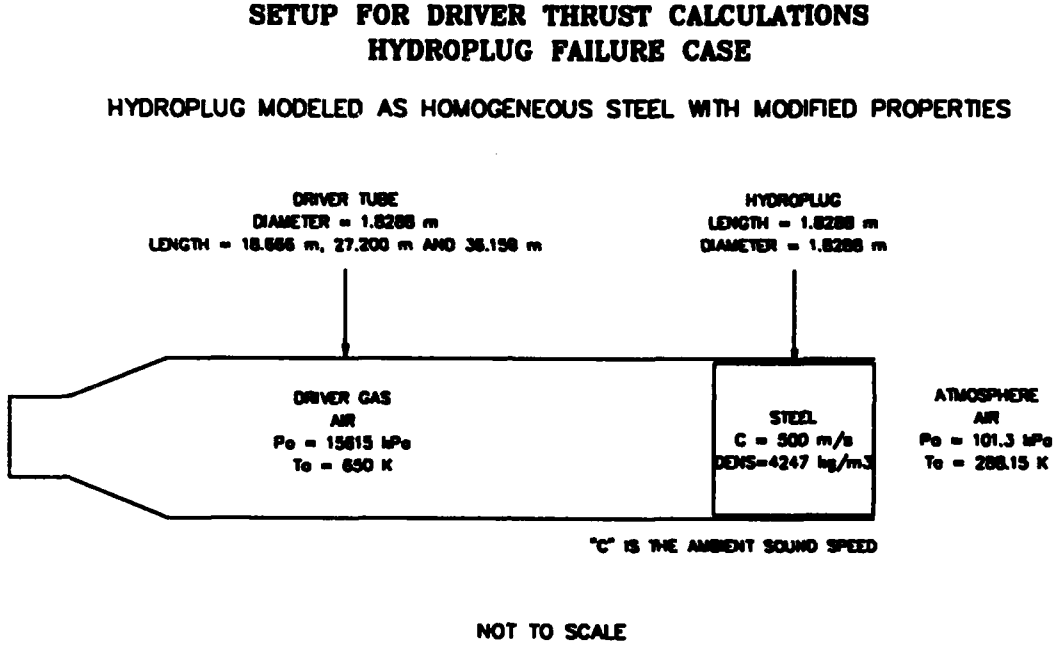

Figure 14. Computational Model for Steel Plug Setup

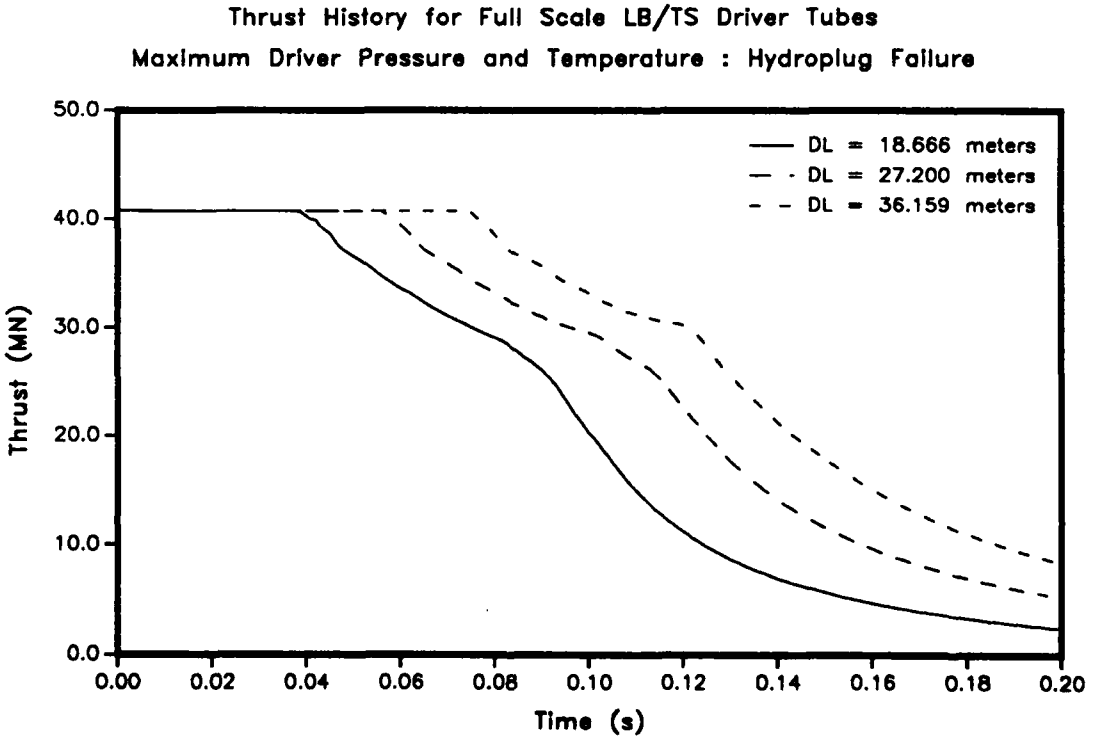

Figure 15. Thrust Histories for Steel Plug Setup

V. Summary

Calculations have been performed to determine the thrust resulting from the release of high pressure gas from various lengths of driver tubes in the proposed Large Blast/Thermal Simulator. In all calculations, the maximum allowable driver gas pressure and temperature were used so that the maximum expected thrust histories would be obtained. The thrust histories were first calculated for the normal operation of the shock tube using four unique lengths of driver tube.

Thrust histories were also calculated for the case in which a driver volume adjusting device (hydroplug) failed. This event would cause the thrust to act in the opposite direction as the normal operation case. The calculations for the plug failure case were performed for three different driver lengths. Several iterations were performed on these calculations, each successive calculation more accurate than the last.

Using the results of this study, the support structure for the driver tubes of the LB/TS can be designed in such a way that the driver tubes will be sufficiently restrained during the operation of the facility.

References

1. Pearson, R.J., Opalka, K.O. and Hisley, D.M., "Design Studies of Drivers for the US Large Blast/Thermal Simulator," Proceedings of the 9^{th} International Symposium on the Military Applications of Blast Simulation, 23-27 September 1985, Atomic Weapons Research Establishment Foulness, Southend-on-Sea, Essex, England SS3 9XE.

2. Fry, M.A., Durret, R.E., Ganong, G.P., Matuska, D.A., Stucker, M.D., Chambers, B.S., Needham, C.E. and Westmoreland, C.D., "The HULL Hydrodynamics Computer Code," US Air Force Weapons Laboratory Technical Report 76-183, September 1977.

3. The Ralph M. Parsons Company, "Large Blast/Thermal Simulator Design Analysis," 100 W. Walnut St., Passadena, California 91124, 2 August 1990.

INTENTIONALLY LEFT BLANK.

APPENDIX A: Density Contours for Dense Air Mass Setup

This appendix contains the density contour plots from the hydroplug failure calculation which used a dense air mass to model the hydroplug. In the discussion of this calculation, the dense air mass was described as having experienced a great deal of diffusion as a result of the pressure imbalance across the hyrdoplug. The following figures illustrate this diffusion. In all the figures, the axis of symmetry of the driver tube runs vertically with the high pressure driver gas below the hydroplug and the ambient atmosphere above the hydroplug. The driver tubes in the LB/TS are very long relative to their diameter. For this reason the radial and axial lengths are drawn to different scales.

Figure A-1 shows the setup at the beginning of the calculation. In this figure, the hydroplug is represented by the horizontal lines running across the page. These horizontal lines represent many different contours of density which are lying on top of one another due to the abrupt changes in density caused by the transitions from driver gas to hydroplug to ambient atmosphere. The following figures show the hydroplug as it is accelerated out of the driver tube and into the surrounding atmosphere. As the figures progress, one can see that as the hydroplug is accelerated it is also beginning to experience diffusion. This diffusion advances as in each successive picture, the contours grow farther apart. By 120 ms the diffusion has progressed to the point where only the bottom two contours are visible. The remainder of the hydroplug has spread to the point that it is no longer in the picture.

These figures illustrate that modeling the hydroplug with a dense air mass provides an improvement in the calculation of thrust histories over the simple discontinuity case. However, the diffusion of the dense air mass was enough that further investigation should be performed to provide a model which more accurately describes the response of the hydroplug.

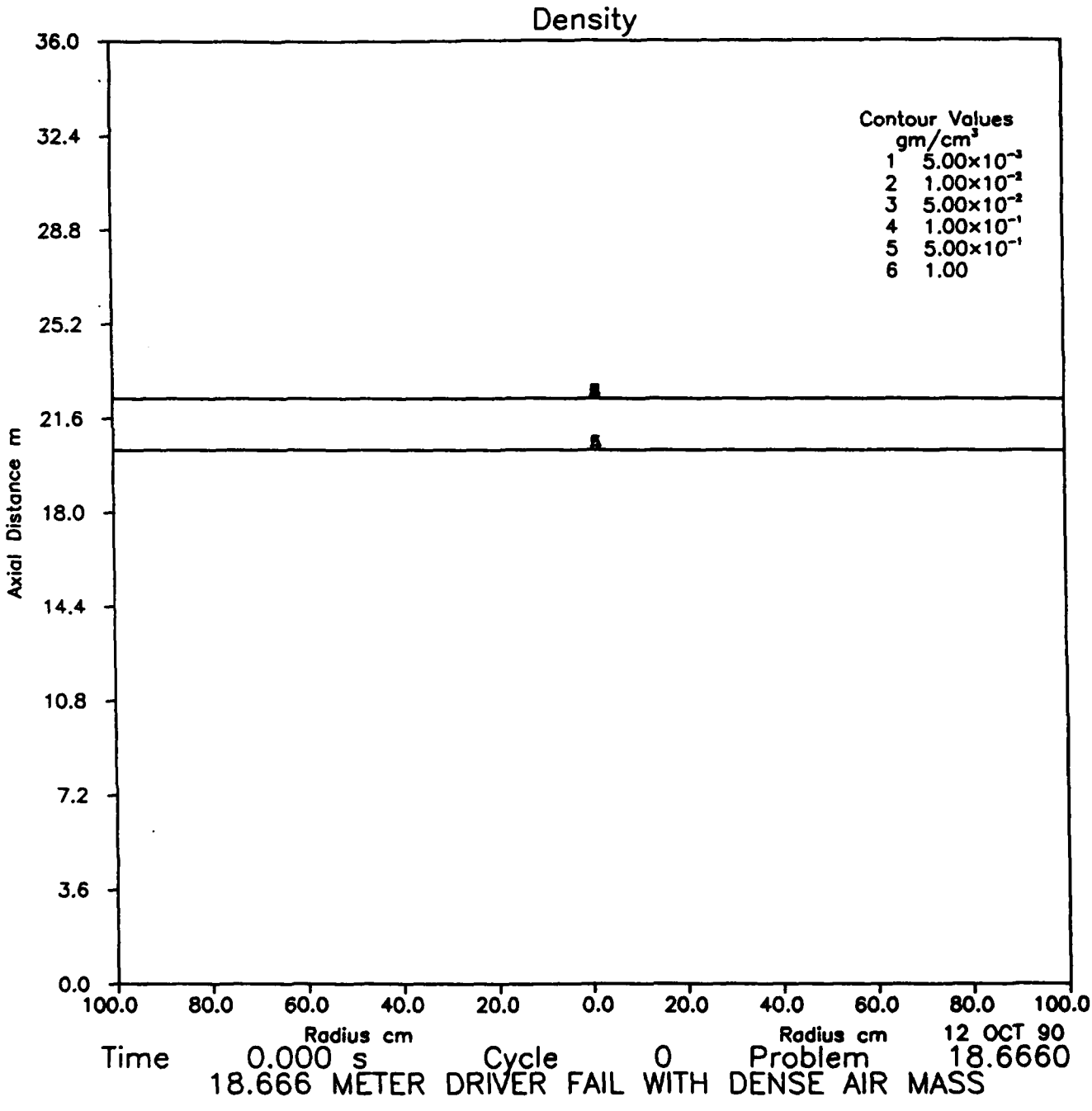

Figure A-1: Dense Air Mass at 0.0 ms

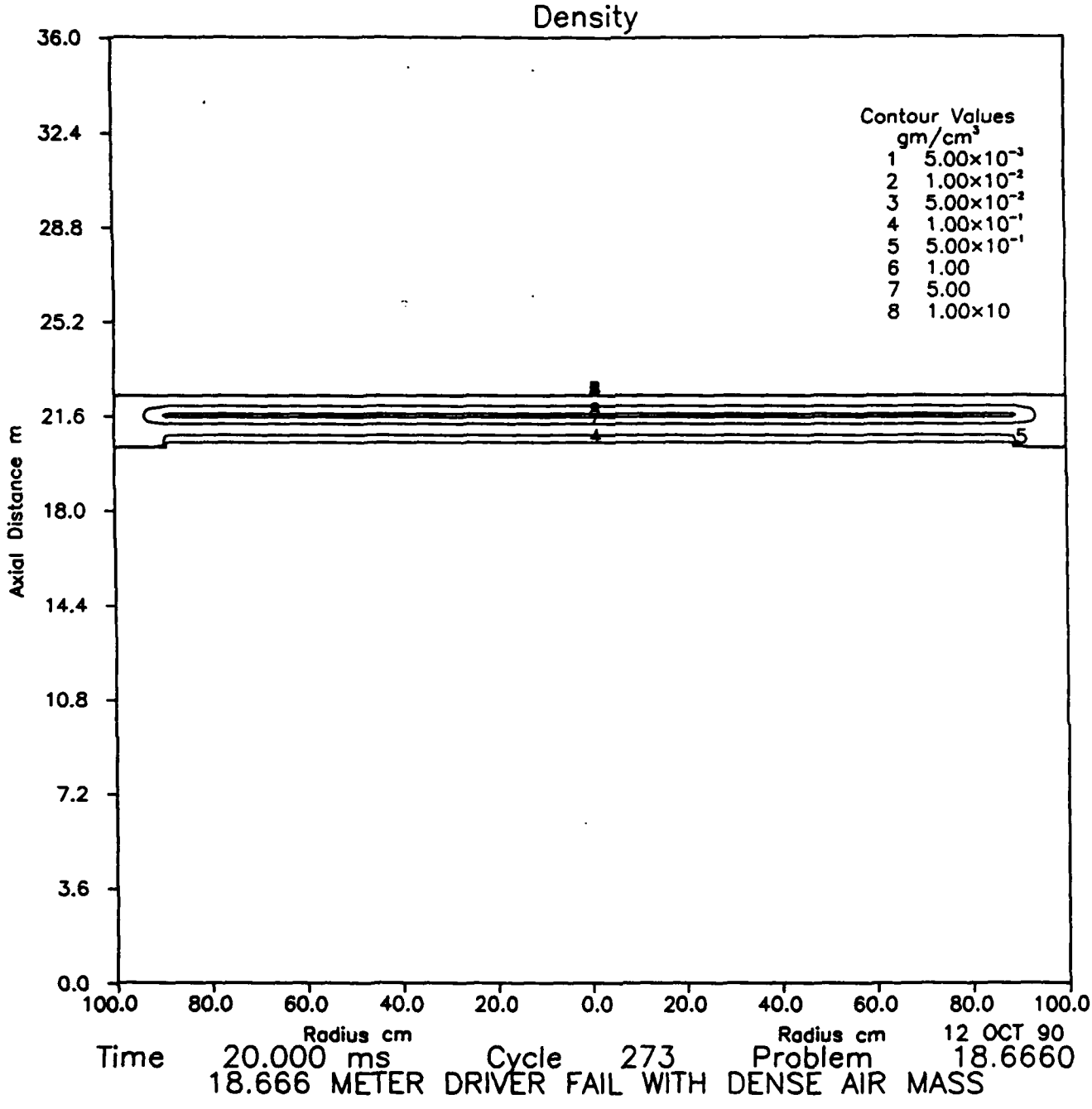

Figure A-2: Dense Air Mass at 20.0 ms

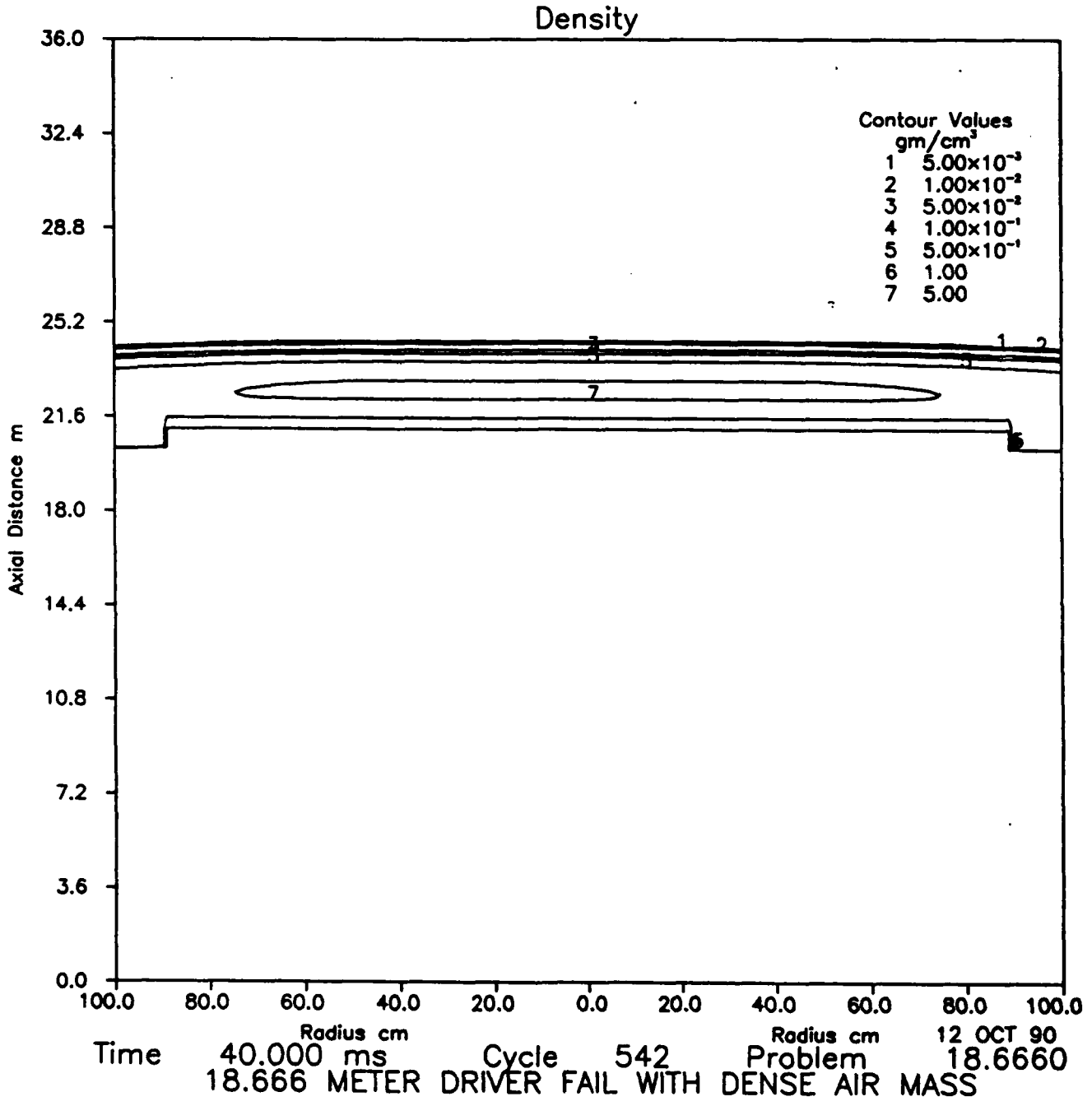

Figure A-3: Dense Air Mass at 40.0 ms

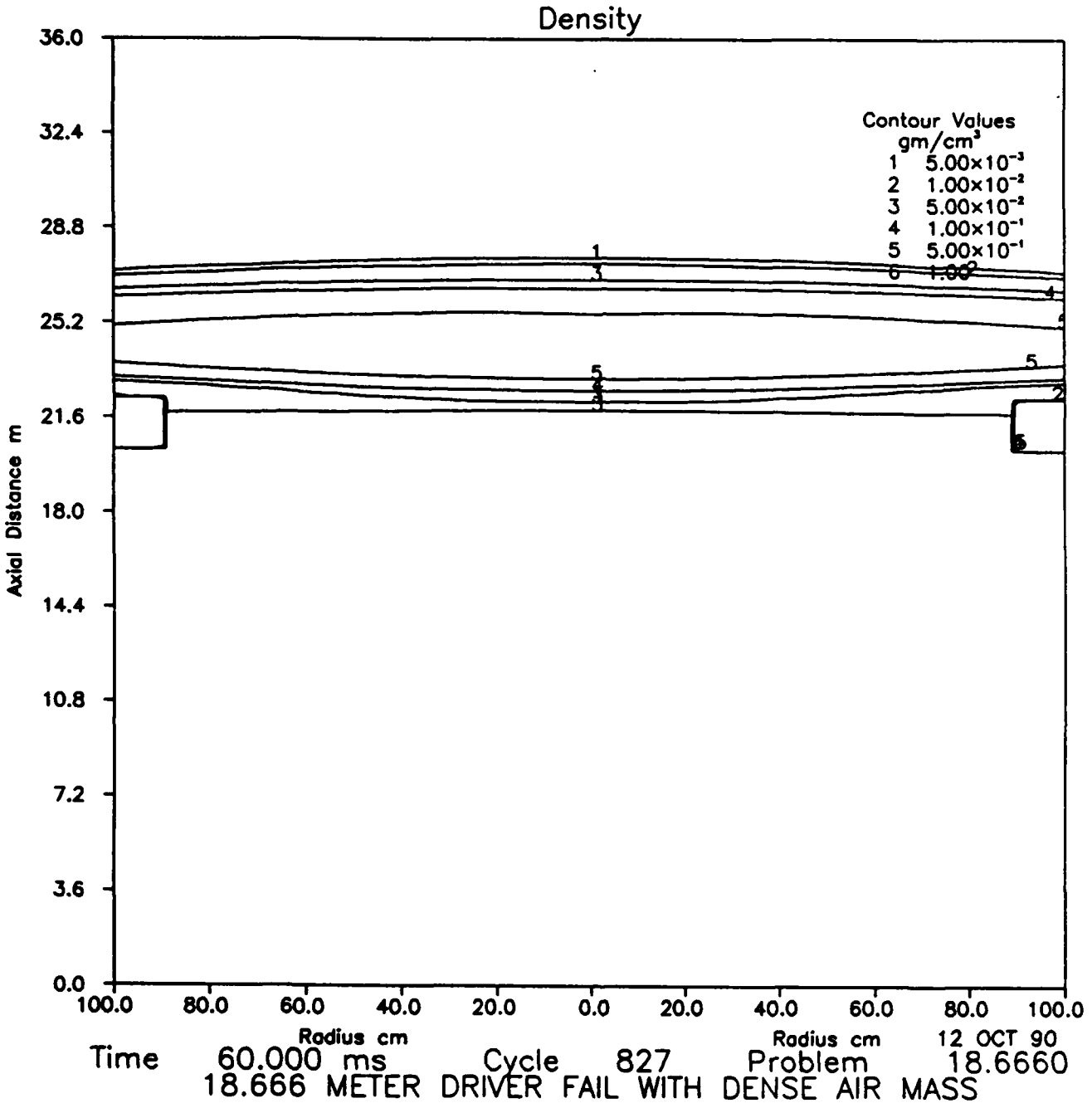

Figure A-4: Dense Air Mass at 60.0 ms

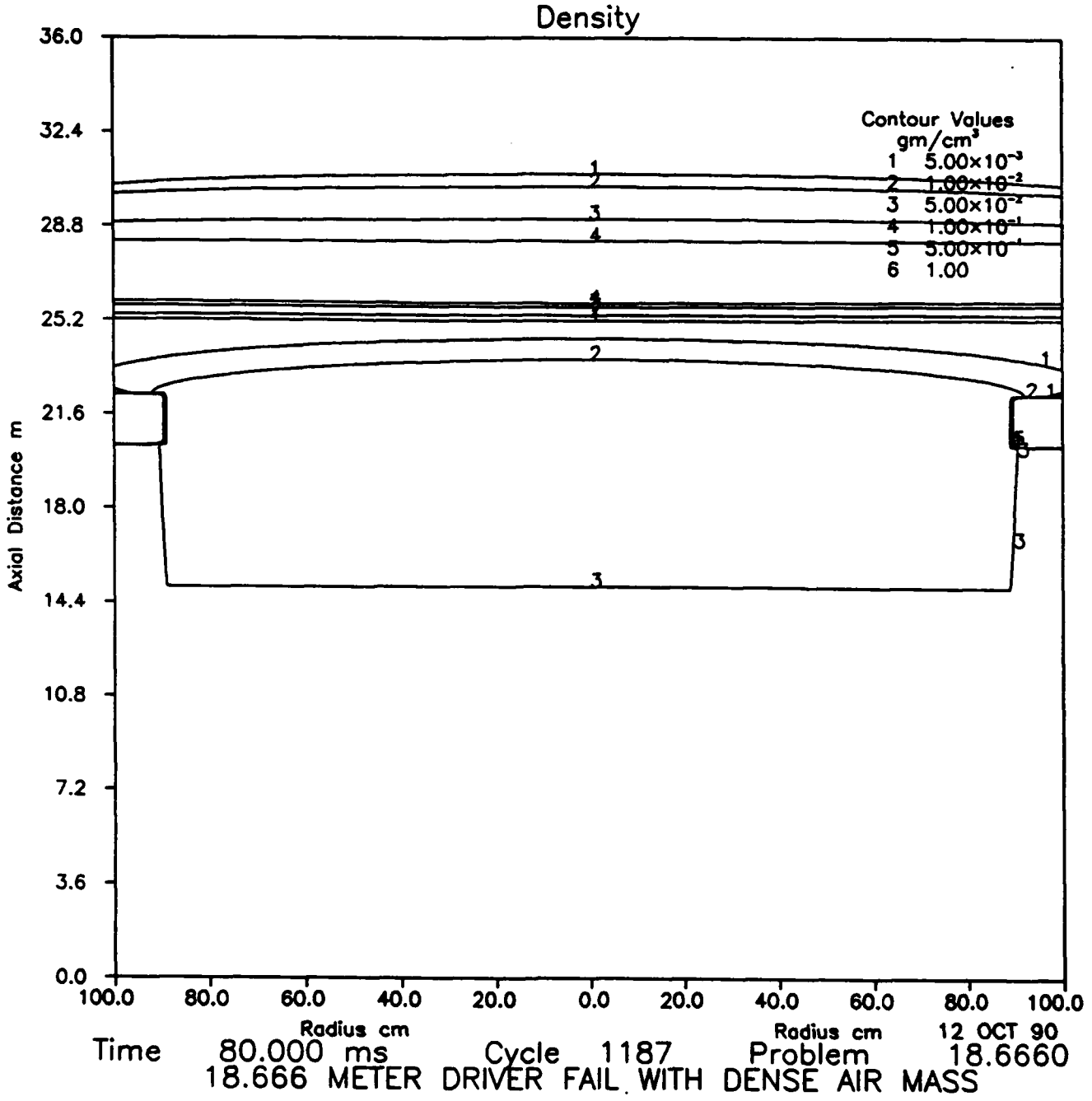

Figure A-5: Dense Air Mass at 80.0 ms

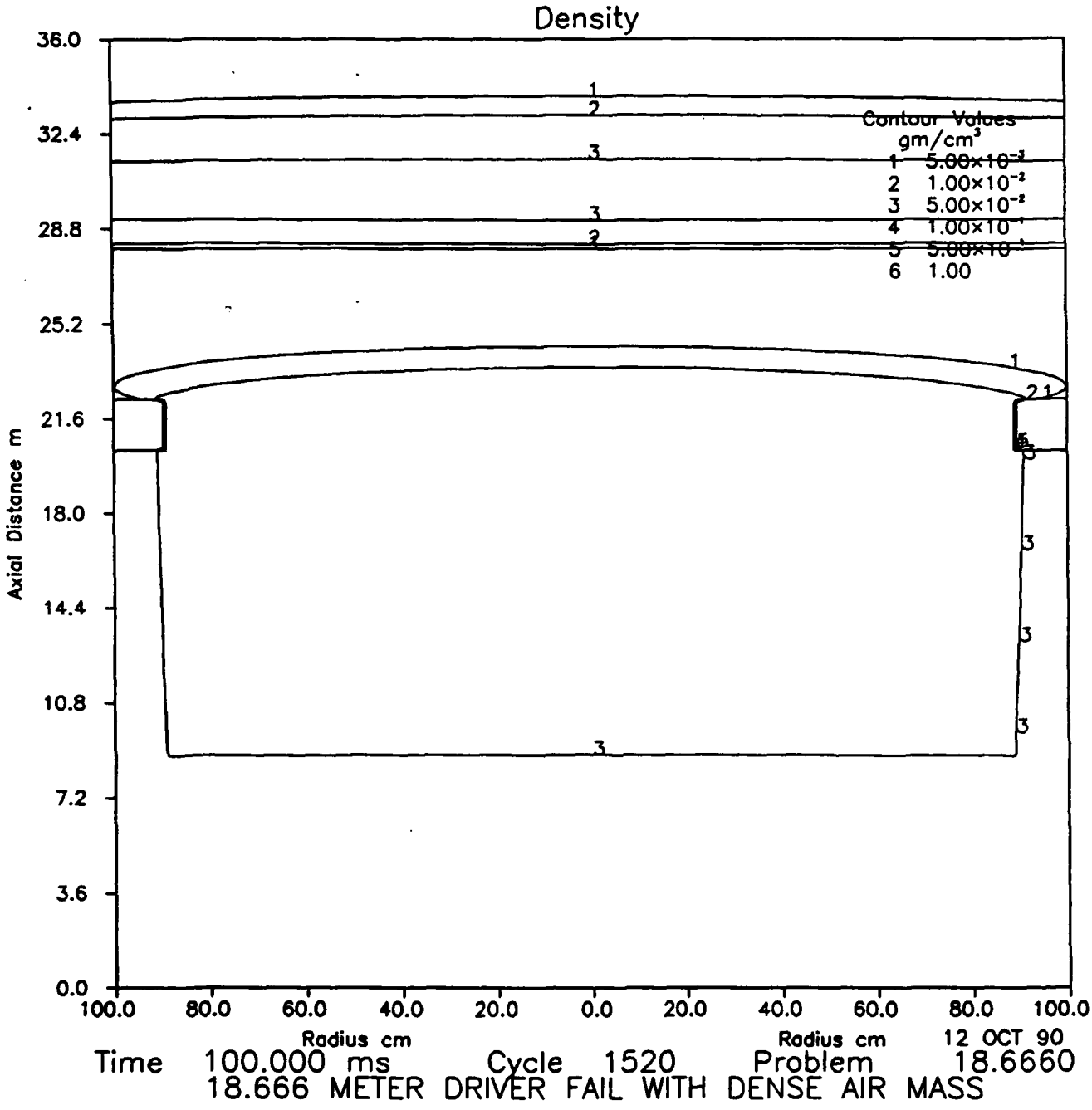

Figure A-6: Dense Air Mass at 100.0 ms

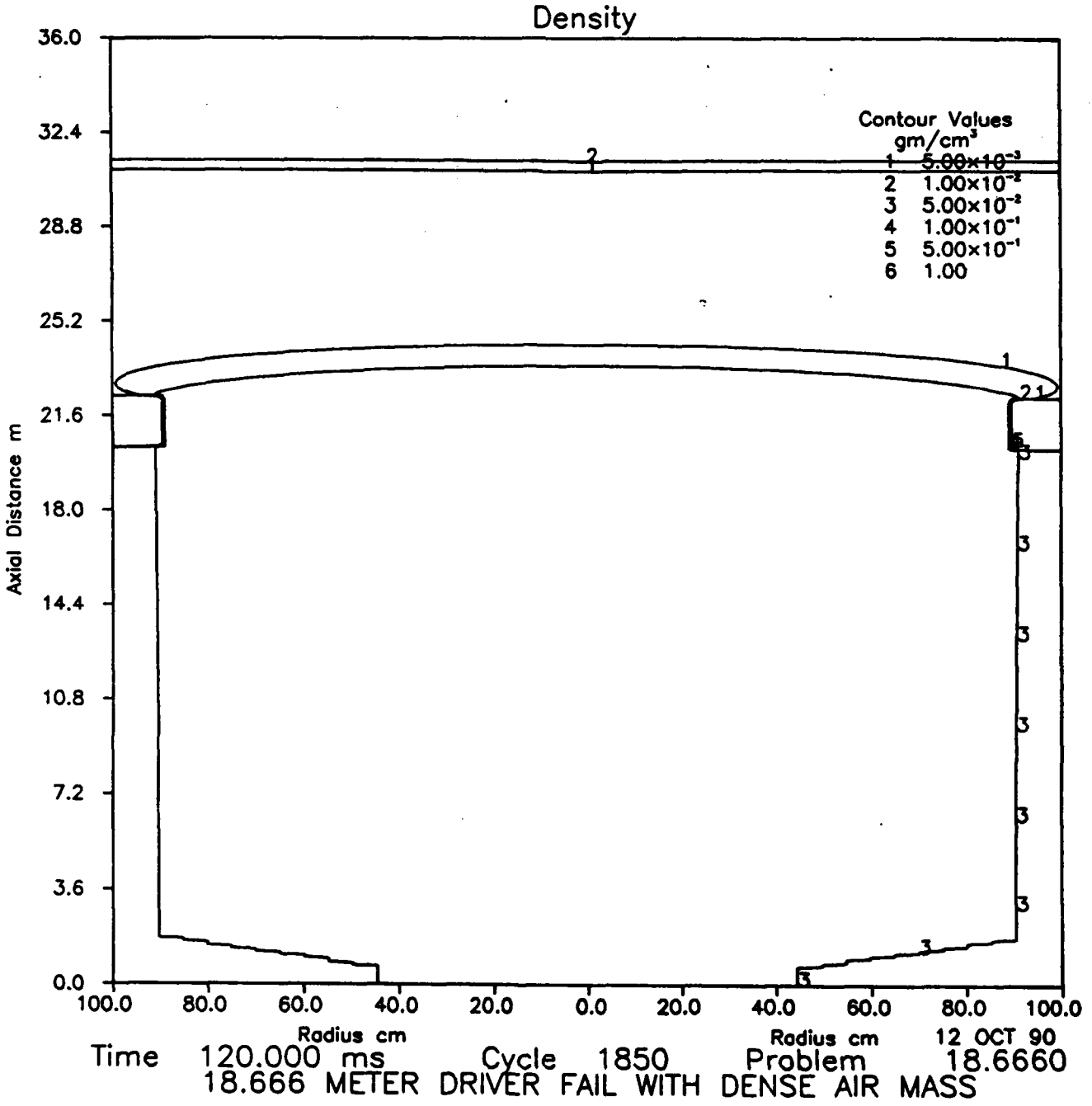

Figure A-7: Dense Air Mass at 120.0 ms

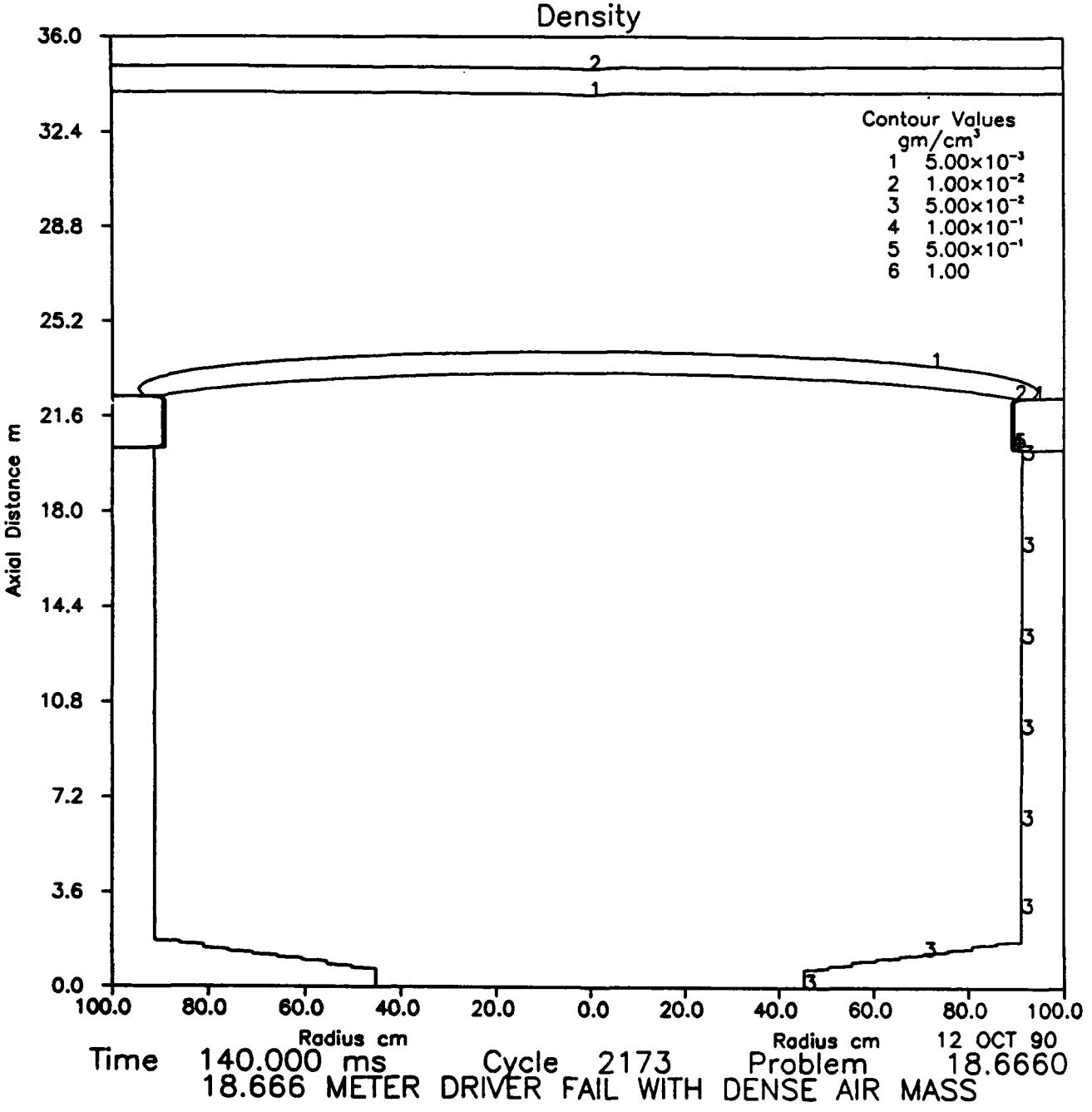

Figure A-8: Dense Air Mass at 140.0 ms

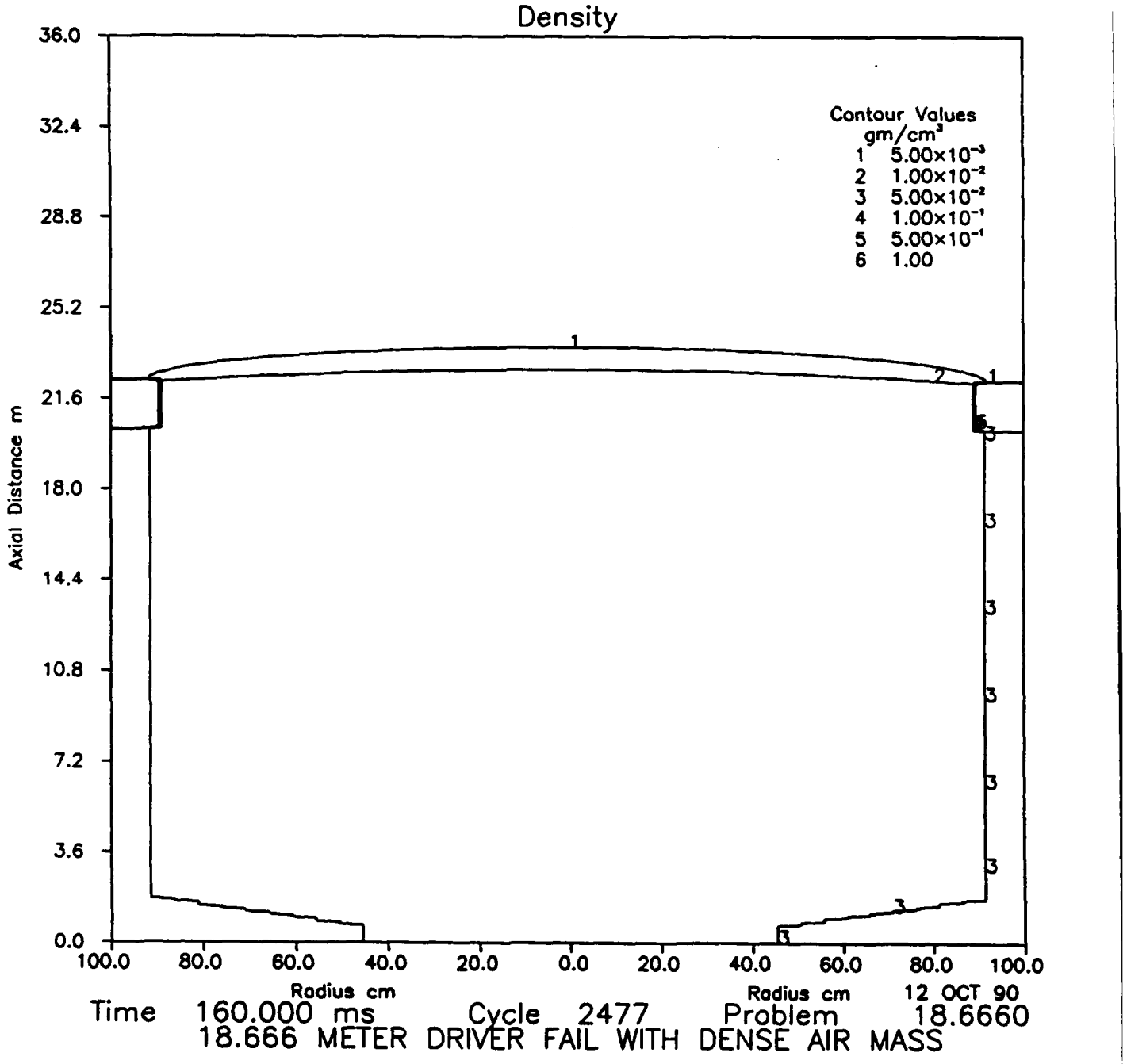

Figure A-9: Dense Air Mass at 160.0 ms

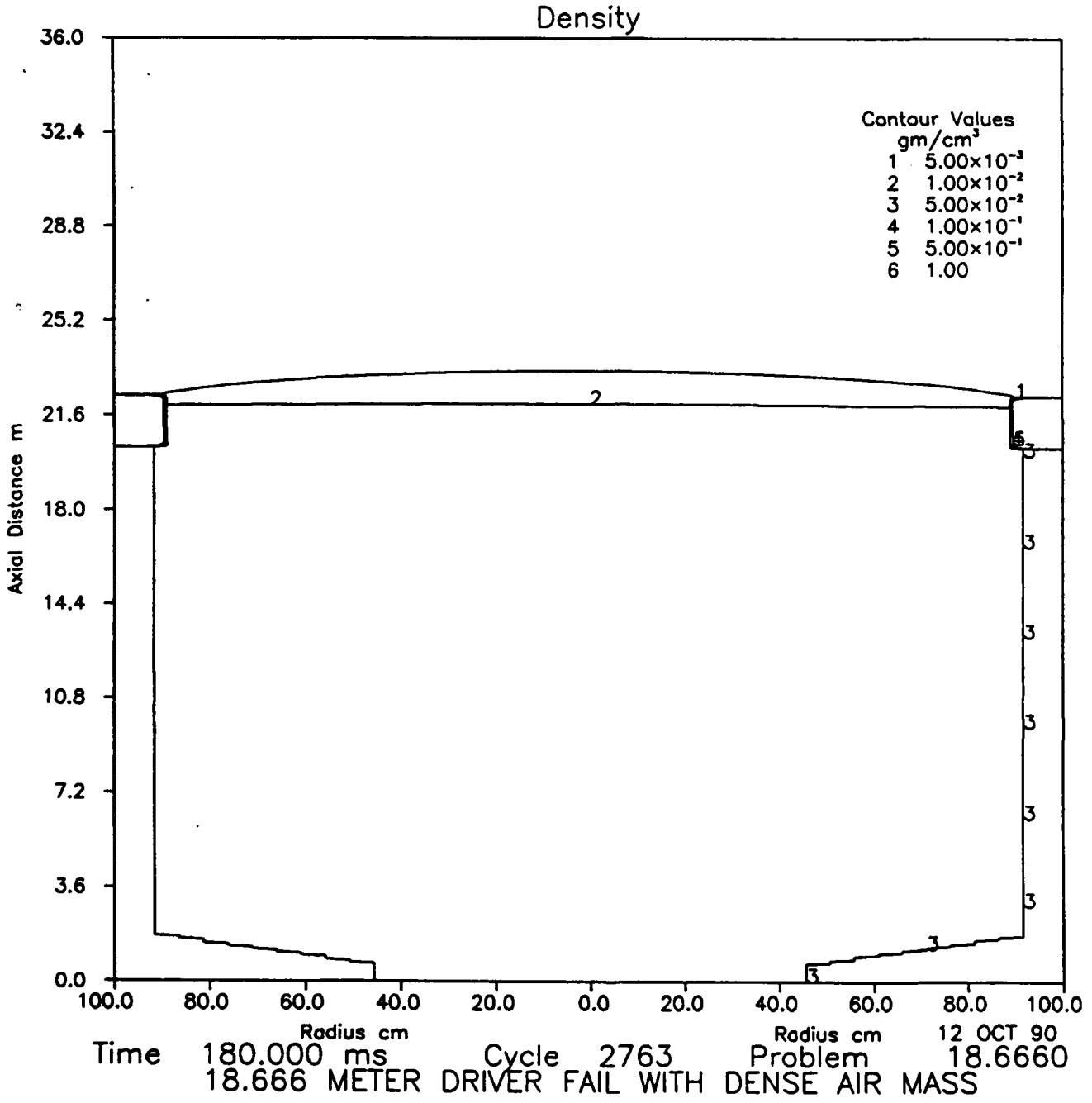

Figure A-10: Dense Air Mass at 180.0 ms

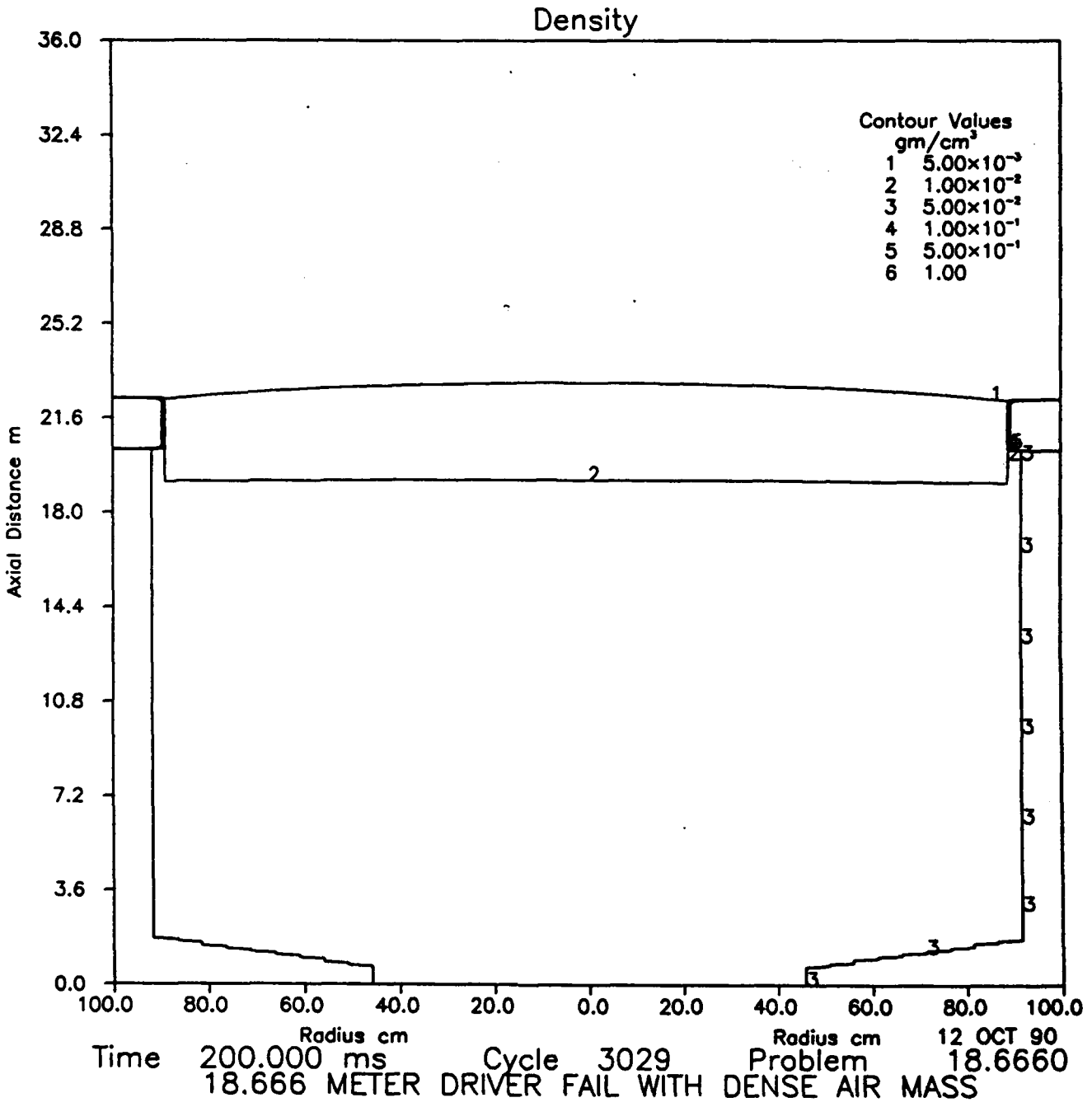

Figure A-11: Dense Air Mass at 200.0 ms

INTENTIONALLY LEFT BLANK.

APPENDIX B: Density Contours for Steel Plug Setup

This appendix contains the density contour plots from the hydroplug failure calculation which used a block of homogeneous steel with modified properties to model the hydroplug. This calculation was performed as an attempt to improve on the results obtained from the calculation which modeled the hydroplug as a dense mass of air.

As seen in Figure A-1, the system at the beginning of the calculation can be seen in Figure B-1. In this figure the hydroplug is represented by the horizontal lines running across the plot. The subsequent figures show the displacement of the hydroplug caused by the high pressure driver gas. By comparing plots in Appendix B with plots in Appendix A for the same points in time, one can see that the hydroplug, when modeled as a steel plug, experienced much less diffusion than the dense air mass case. The improved accuracy of the steel plug calculation is most evident when comparing Figure A-8 to Figure B-8. Both these figures represent the system at a point in time 140 *ms* into the calculation. In Figure A-8, most of the hydroplug has exited the picture and only the bottom remains visible. In Figure B-8, the hydroplug is not only visible, but it is still roughly intact although it has undergone some deformation. The limited diffusion of the hydroplug is evident in all the figures in Appendix B. Based on the results of this calculation it was concluded that these results provided an accurate representation of the loads placed on the driver tubes of the LB/TS should a hydroplug failure occur.

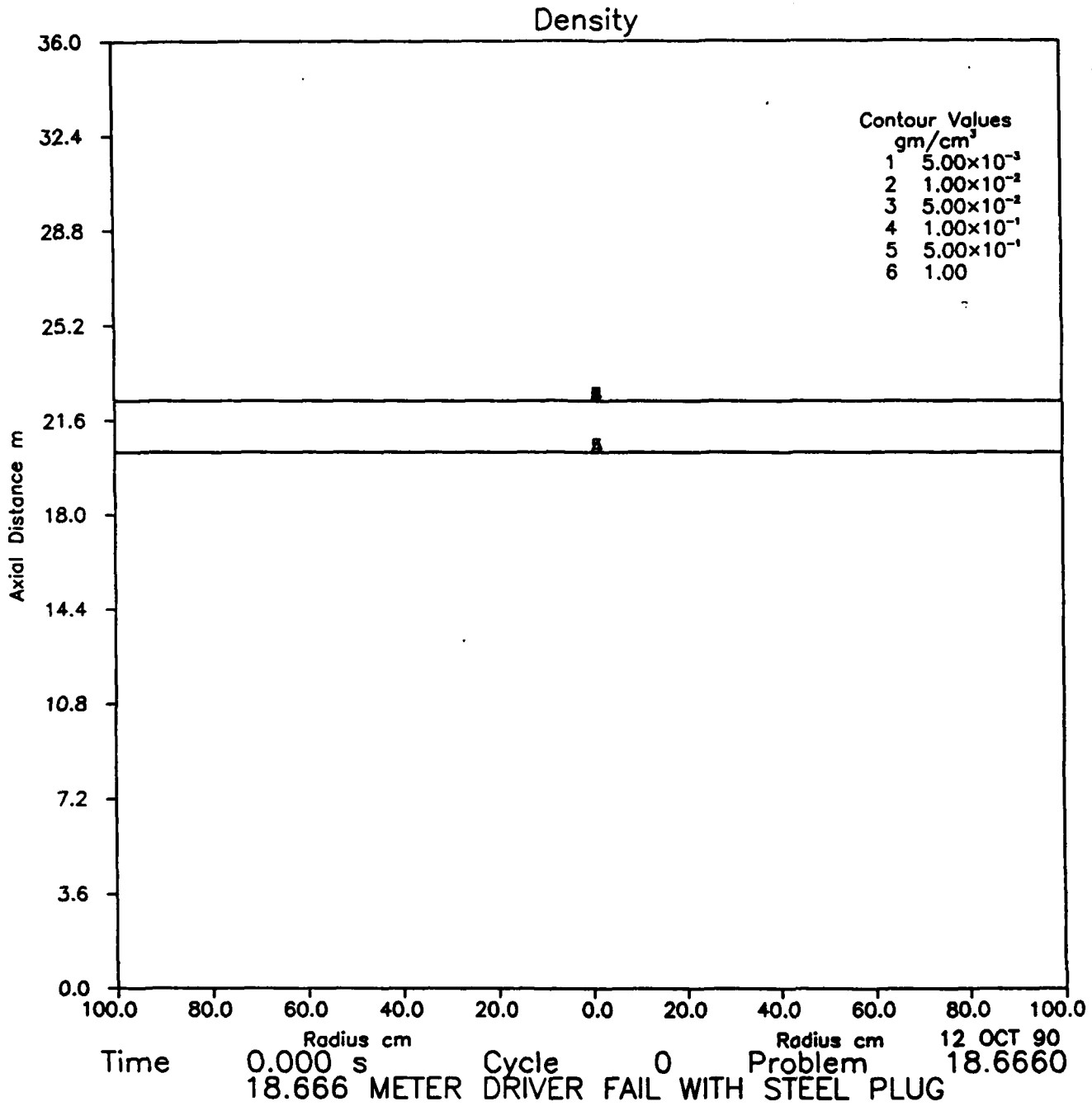

Figure B-1: Steel Plug at 0.0 ms

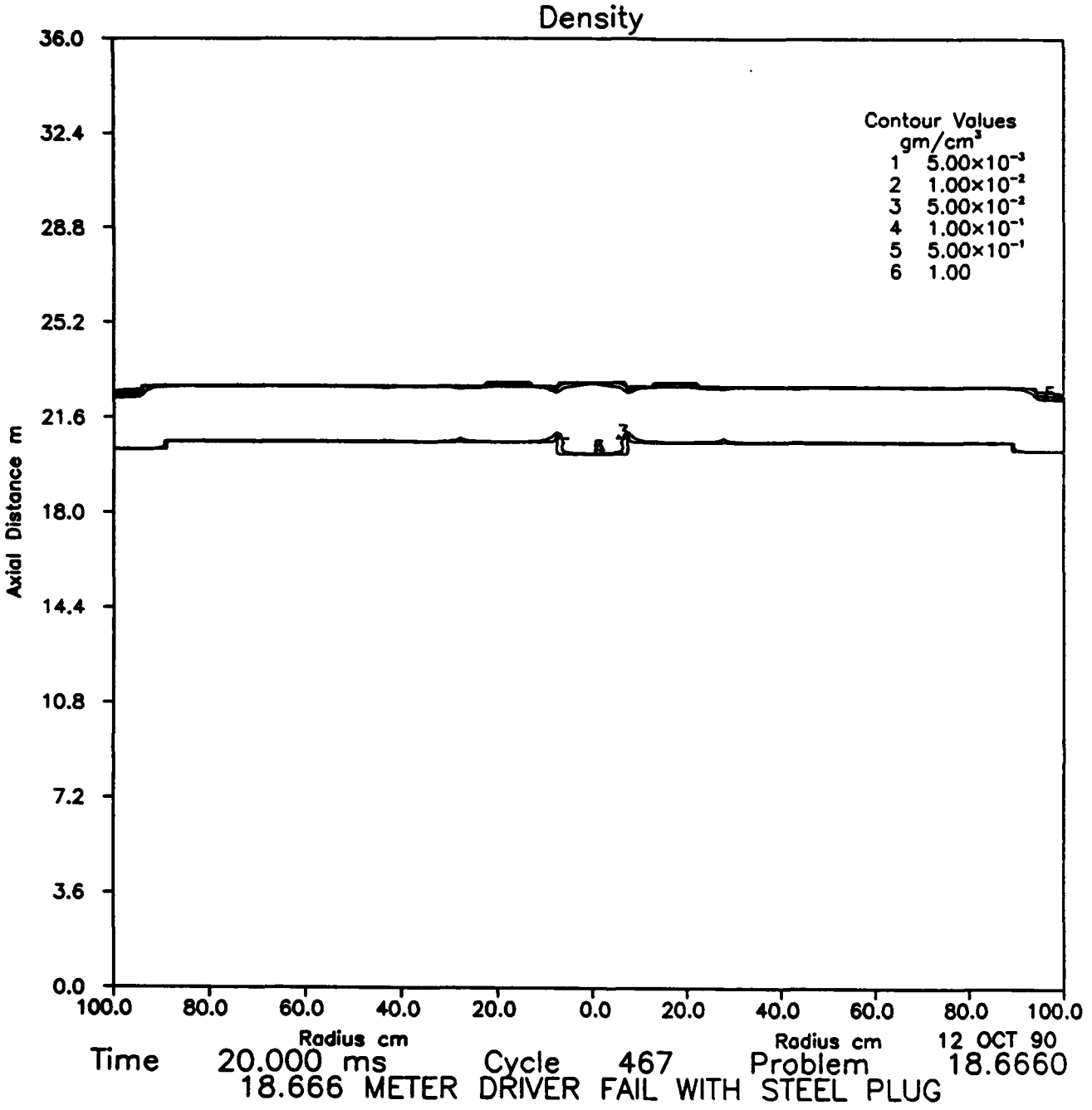

Figure B-2: Steel Plug at 20.0 ms

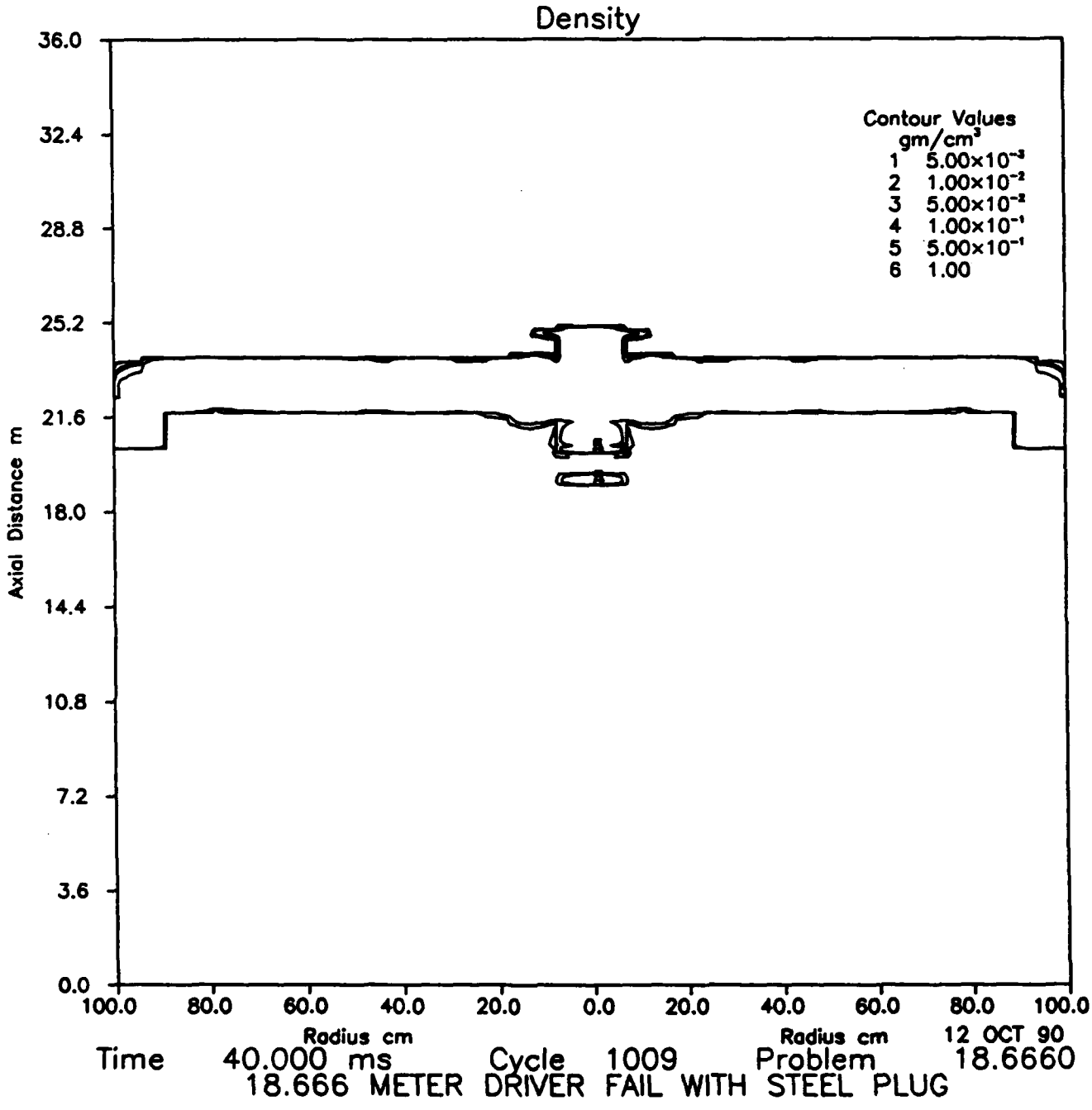

Figure B-3: Steel Plug at 40.0 ms

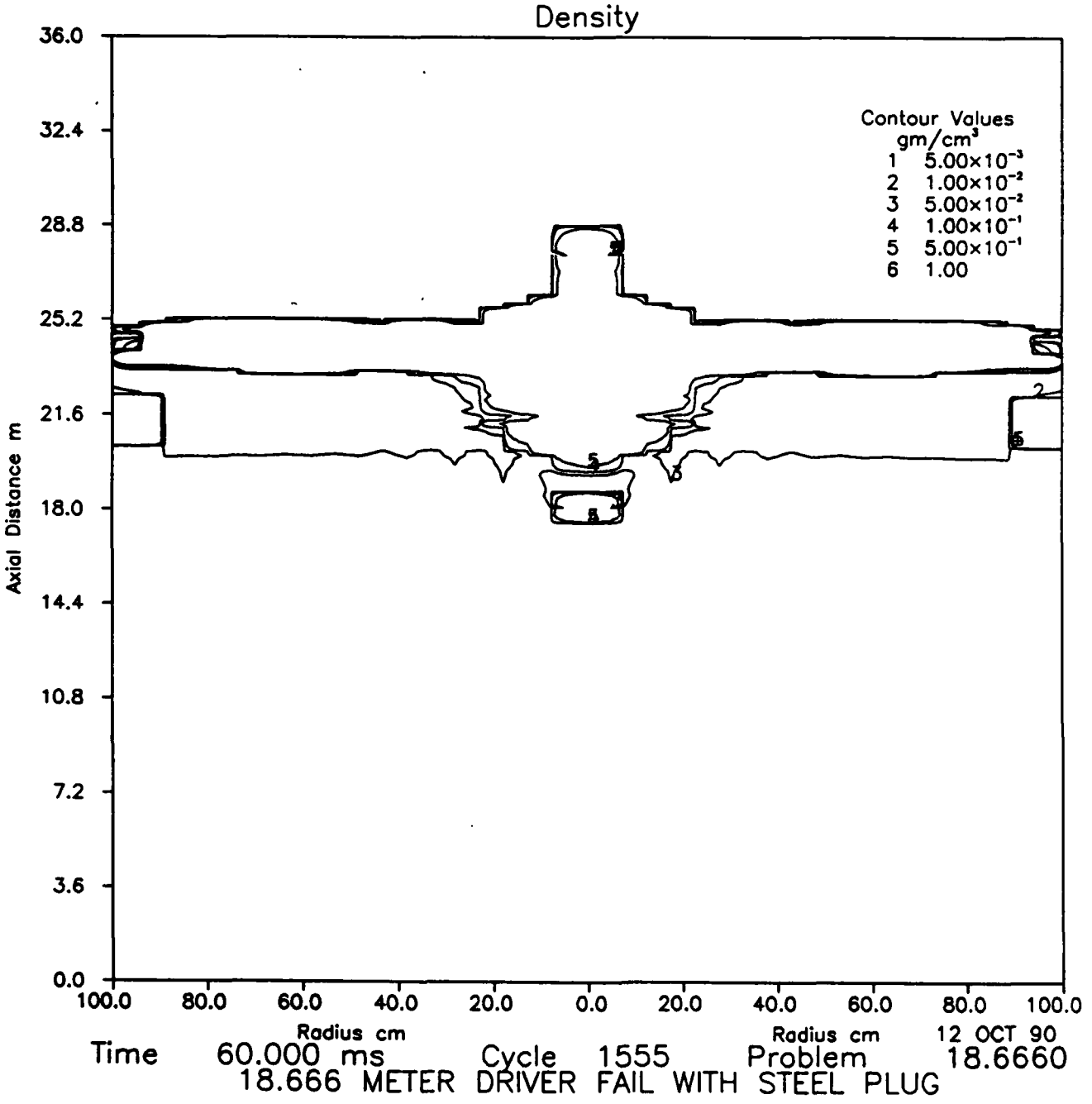

Figure B-4: Steel Plug at 60.0 ms

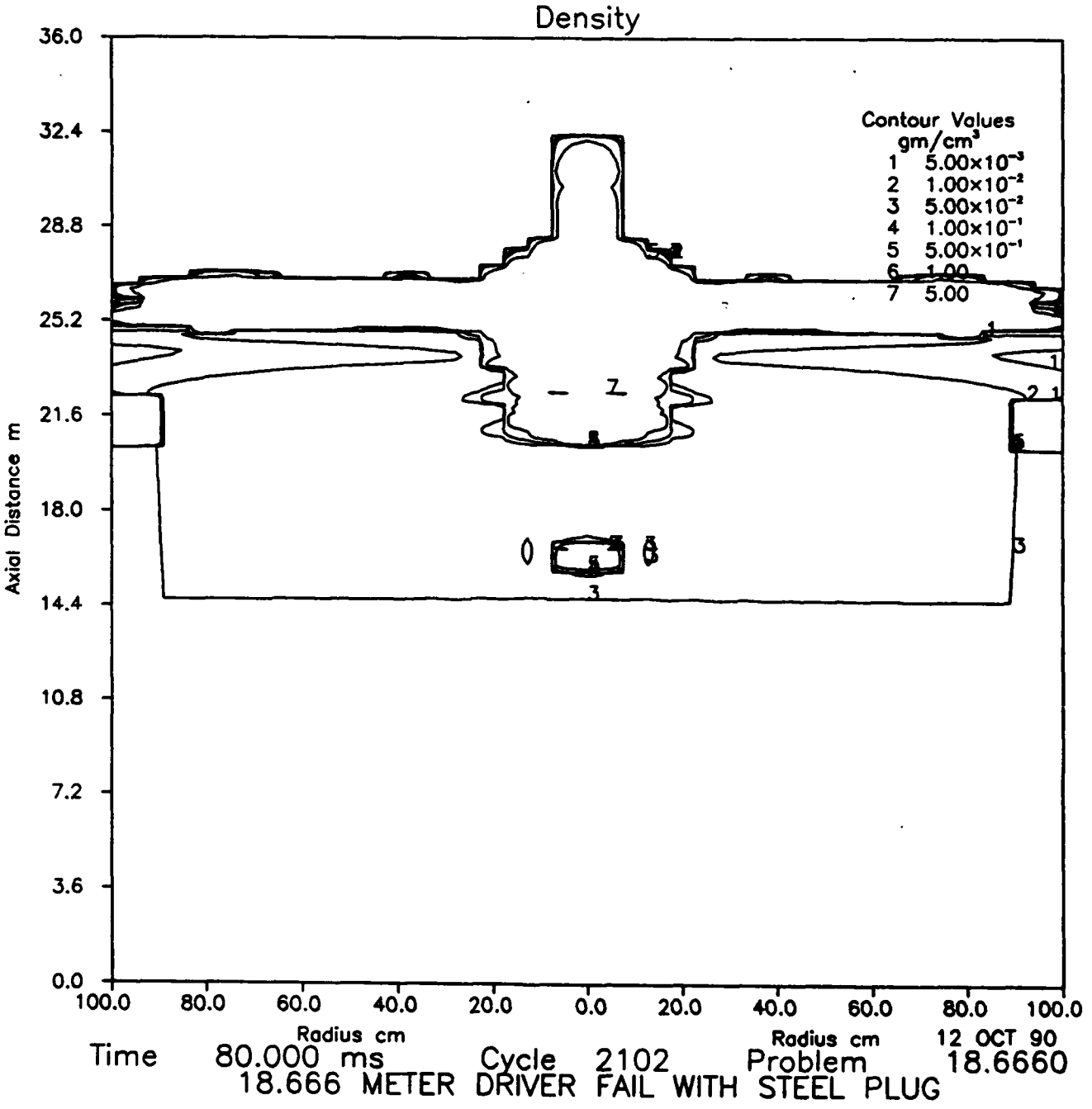

Figure B-5: Steel Plug at 80.0 ms

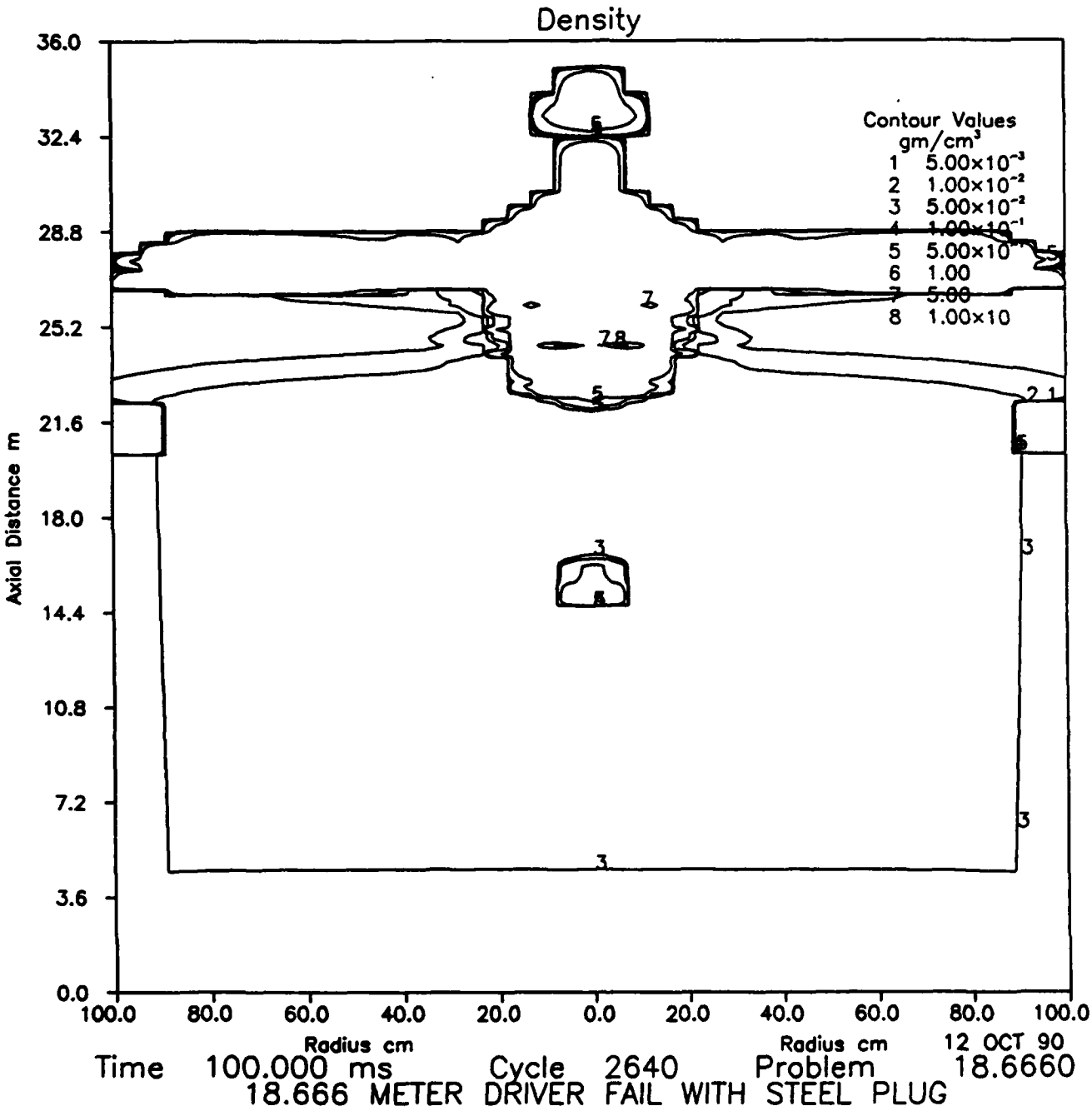

Figure B-6: Steel Plug at 100.0 ms

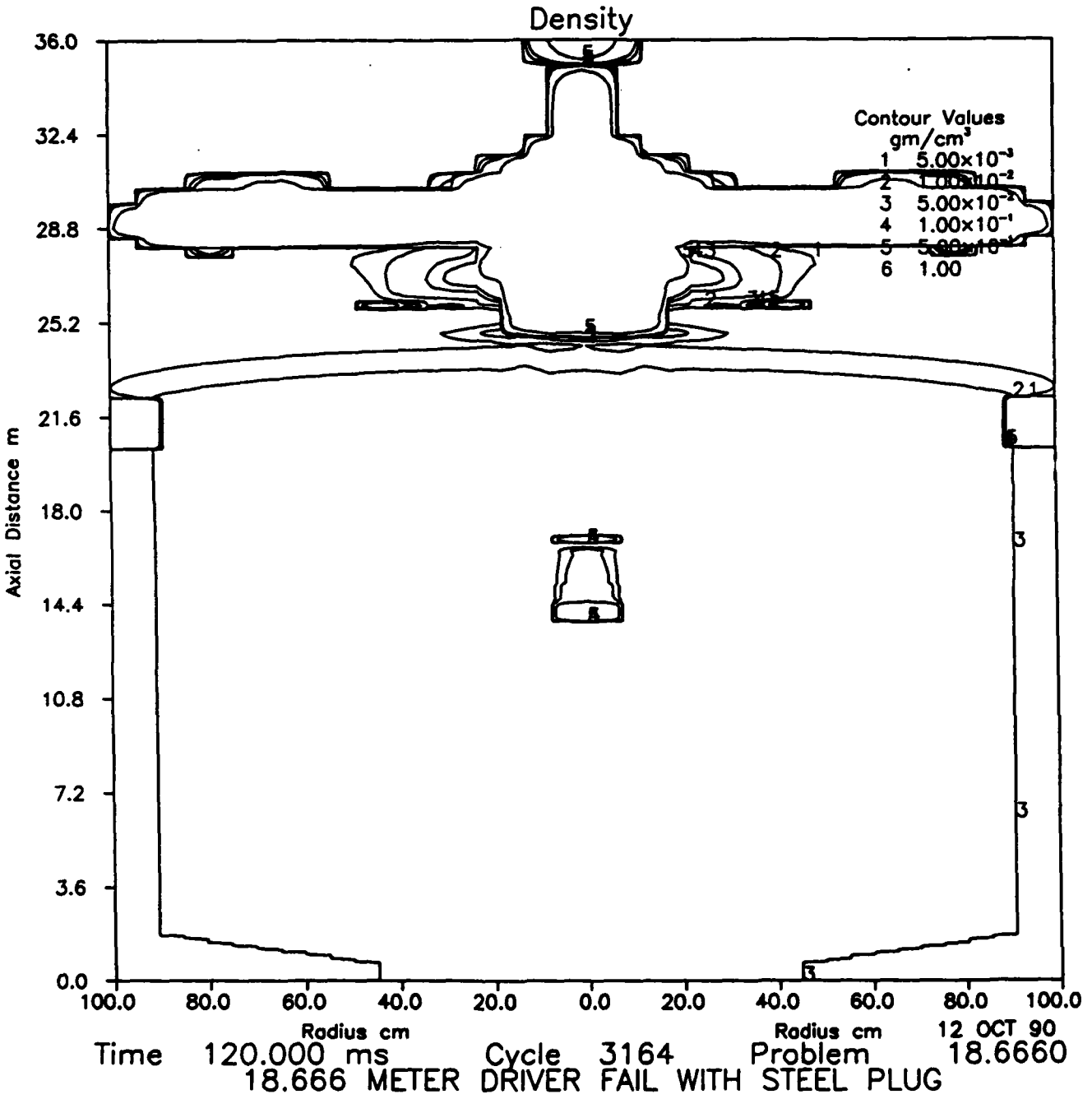

Figure B-7: Steel Plug at 120.0 ms

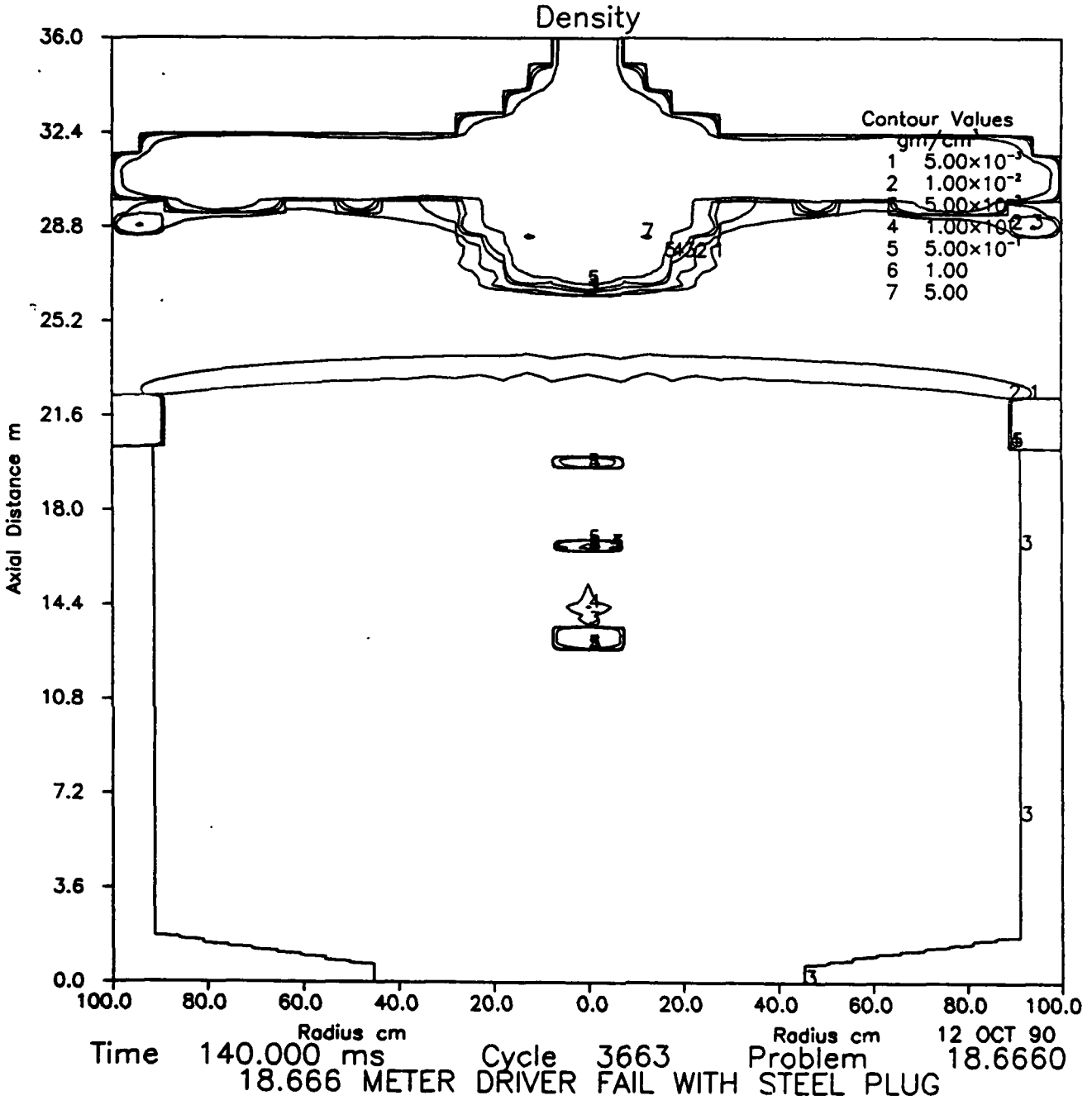

Figure B-8: Steel Plug at 140.0 ms

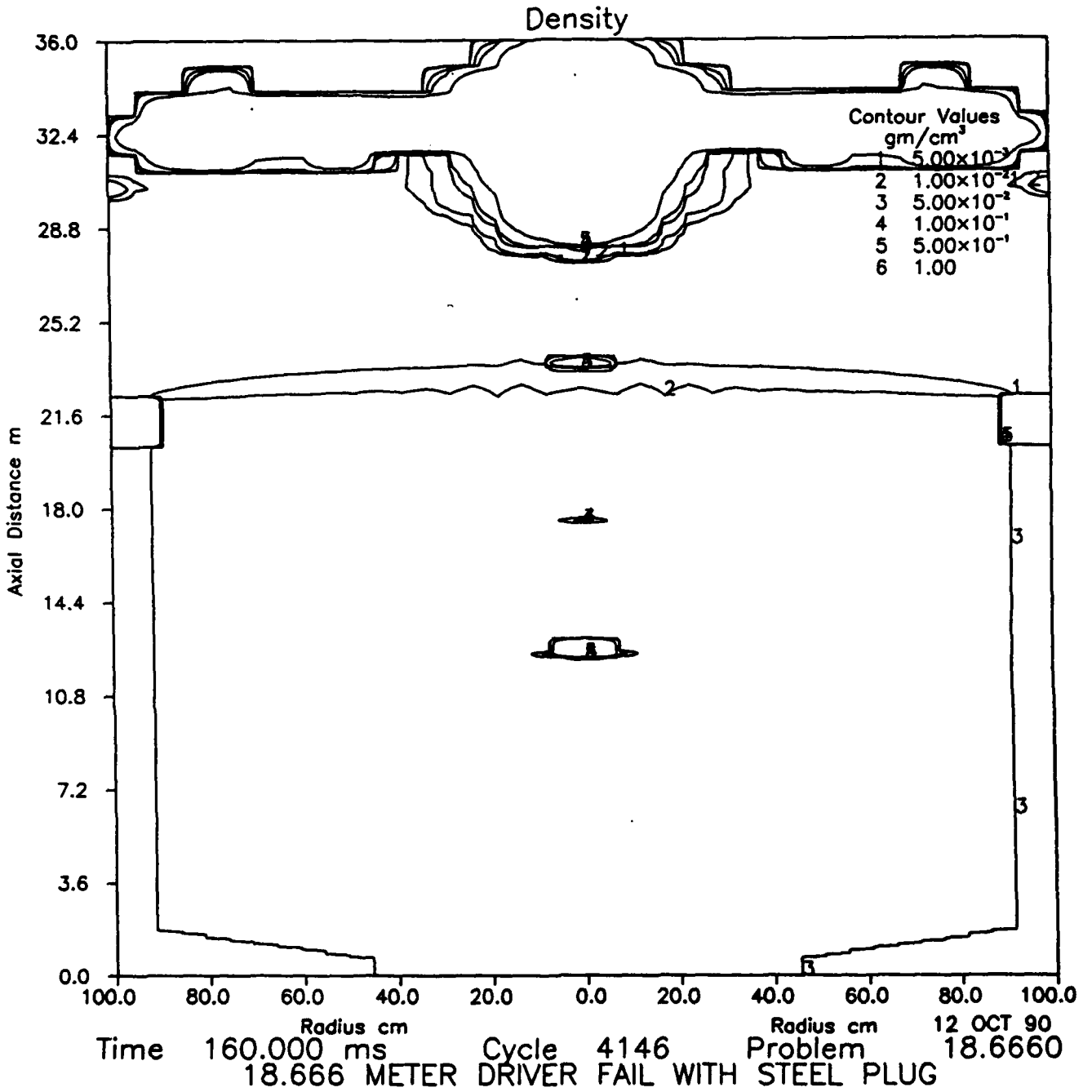

Figure B-9: Steel Plug at 160.0 ms

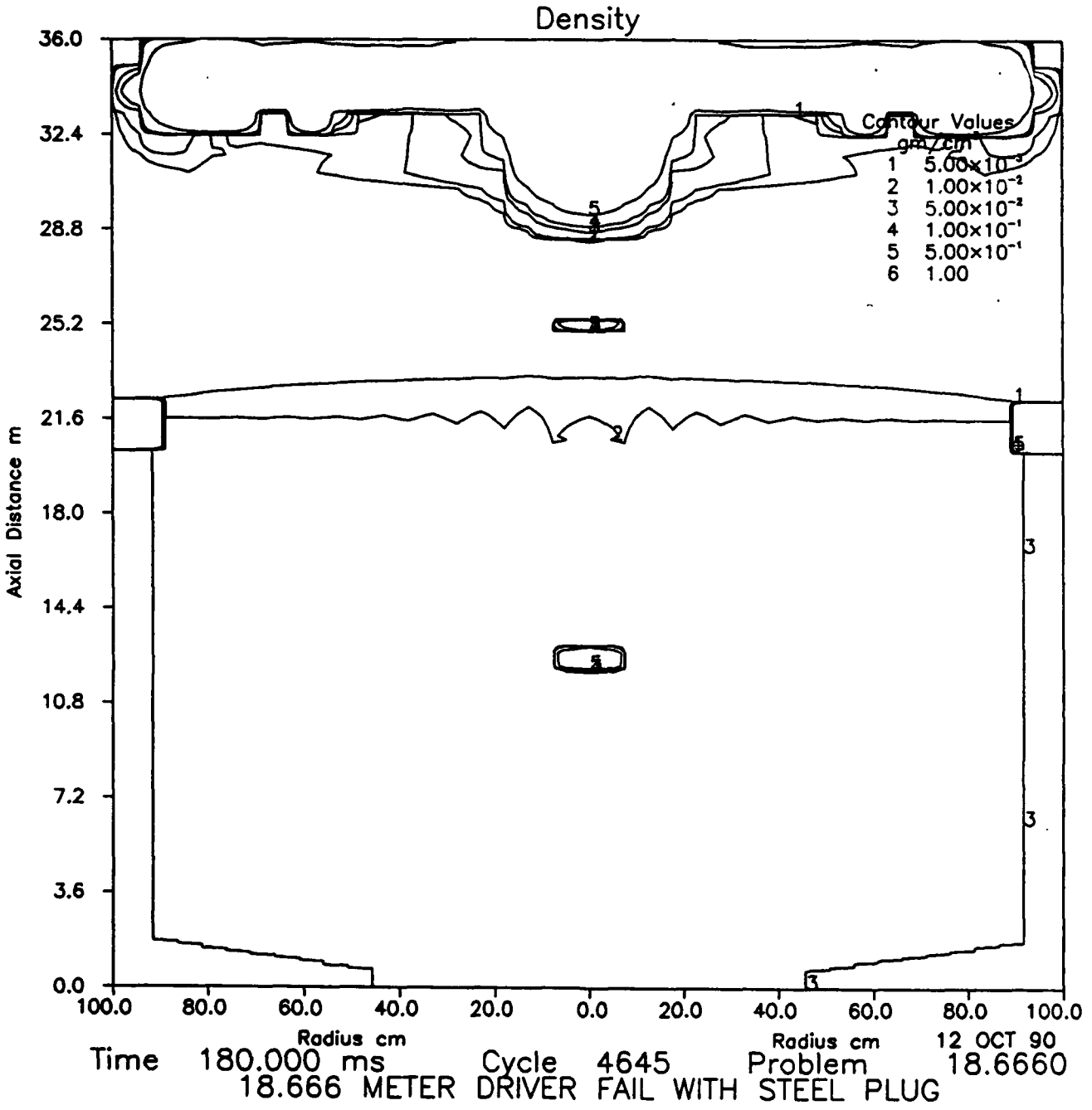

Figure B-10: Steel Plug at 180.0 ms

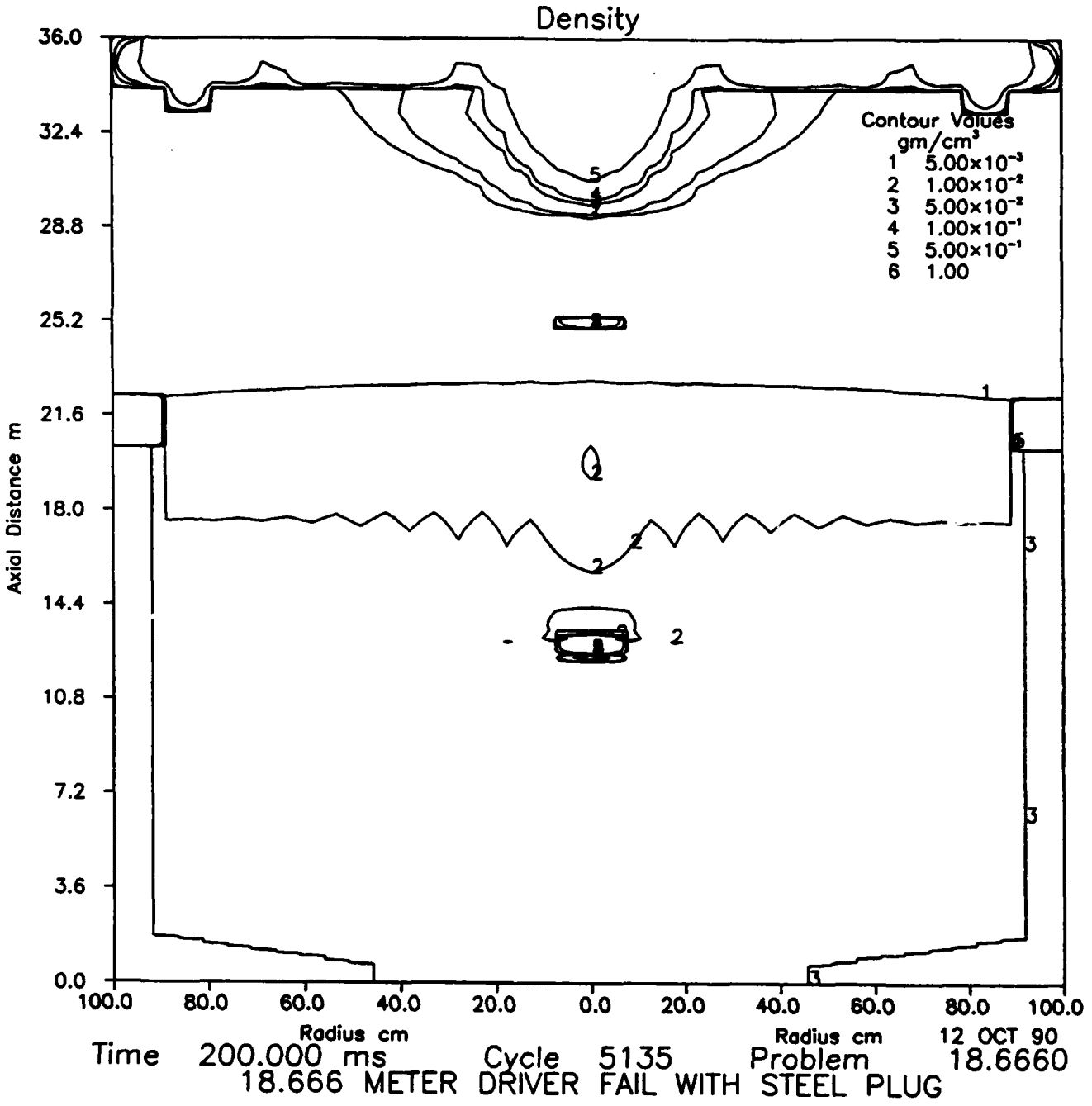

Figure B-11: Steel Plug at 200.0 ms

INTENTIONALLY LEFT BLANK.

No of Copies	Organization
2	Administrator Defense Technical Info Center ATTN: DTIC-DDA Cameron Station Alexandria, VA 22304-6145
1	HQDA (SARD-TR) WASH DC 20310-0001
1	Commander U.S. Army Materiel Command ATTN: AMCDRA-ST 5001 Eisenhower Avenue Alexandria, VA 22333-0001
1	Commander U.S. Army Laboratory Command ATTN: AMSLC-DL 2800 Powder Mill Road Adelphi, MD 20783-1145
2	Commander U.S. Army Armament Research, Development, and Engineering Center ATTN: SMCAR-IMI-I Picatinny Arsenal, NJ 07806-5000
2	Commander U.S. Army Armament Research, Development, and Engineering Center ATTN: SMCAR-TDC Picatinny Arsenal, NJ 07806-5000
1	Director Benet Weapons Laboratory U.S. Army Armament Research, Development, and Engineering Center ATTN: SMCAR-CCB-TL Watervliet, NY 12189-4050
1	Commander U.S. Army Armament, Munitions and Chemical Command ATTN: SMCAR-ESP-L Rock Island, IL 61299-5000
1	Director U.S. Army Aviation Research and Technology Activity ATTN: SAVRT-R (Library) M/S 219-3 Ames Research Center Moffett Field, CA 94035-1000

No of Copies	Organization
1	Commander U.S. Army Missile Command ATTN: AMSMI-RD-CS-R (DOC) Redstone Arsenal, AL 35898-5010
1	Commander U.S. Army Tank-Automotive Command ATTN: AMSTA-TSL (Technical Library) Warren, MI 48397-5000
1	Director U.S. Army TRADOC Analysis Command ATTN: ATRC-WSR White Sands Missile Range, NM 88002-5502
(Class. only)1	Commandant U.S. Army Infantry School ATTN: ATSH-CD (Security Mgr.) Fort Benning, GA 31905-5660
(Unclass. only)1	Commandant U.S. Army Infantry School ATTN: ATSH-CD-CSO-OR Fort Benning, GA 31905-5660
1	Air Force Armament Laboratory ATTN: AFATL/DLODL Eglin AFB, FL 32542-5000
	Aberdeen Proving Ground
2	Dir, USAMSAA ATTN: AMXSY-D AMXSY-MP, H. Cohen
1	Cdr, USATECOM ATTN: AMSTE-TD
3	Cdr, CRDEC, AMCCOM ATTN: SMCCR-RSP-A SMCCR-MU SMCCR-MSI
1	Dir, VLAMO ATTN: AMSLC-VL-D
10	Dir, BRL ATTN: SLCBR-DD-T

No. of
Copies Organization

1 Director of Defense Research & Engineering
ATTN: DD/TWP
Washington, DC 20301

1 Assistant Secretary of Defense (Atomic Energy)
ATTN: Document Control
Washington, DC 20301

1 Chairman
Joint Chiefs of Staff
ATTN: J-5, R&D Division
Washington, DC 20301

2 Deputy Chief of Staff for Operations and Plans
ATTN: Technical Library
Director of Chemical and Nuclear Operations
Department of the Army
Washington, DC 20310

1 Director
Defense Advanced Research Projects Agency
ATTN: Tech Lib
1400 Wilson Boulevard
Arlington, VA 22209

2 Director
Federal Emergency Management Agency
ATTN: Public Relations Office
Technical Library
Washington, DC 20472

1 Director
Defense Intelligence Agency
ATTN: DT-2/Wpns & Sys Div
Washington, DC 20301

1 Director
National Security Agency
ATTN: R15, E. F. Butala
Ft. George G. Meade, MD 20755

No. of
Copies Organization

9 Director
Defense Nuclear Agency
ATTN: CSTI, Tech Lib
DDIR
DFSP, Ullrich
NANS
OPNA
SPSD,
Goering
Rohr
SPTD,
Kennedy
Hrinishin
Washington, DC 20305

3 Commander
Field Command, DNA
ATTN: FCPR
FCTMOF
NMHE, CDR Lund
Kirtland AFB, NM 87115

10 Central Intelligence Agency
DIR/DB/Standard
ATTN: GE-47 HQ
Washington, DC 20505

1 Commandant
Interservice Nuclear Weapons School
ATTN: Technical Library
Kirtland AFB, NM 87115

4 Director
US Army Harry Diamond Laboratories
ATTN: SLCHD-NW-RA,
L. Belliveau
SLCHD-NW-P,
Corrigan
Gwaltney
SLCHD-TA-L, Tech Lib
2800 Powder Mill Road
Adelphi, MD 20783-1197

2 Commander, USACECOM
ATTN: AMSEL-RD
AMSEL-RO-TPPO-P
Fort Monmouth, NJ 07703-5301

No. of Copies	Organization
1	Commander, USACECOM R&D Technical Library ATTN: ASQNC-ELC-I-T, Myer Center Fort Monmouth, NJ 07703-5301
1	Director US Army Laboratory Command USASMO ATTN: SLCSM-SE, J. Orsega 2800 Powder Mill Road Adelphi, MD 20783-1197
1	Director US Army Missile and Space Intelligence Center ATTN: AIAMS-YDL Redstone Arsenal, AL 35898-5500
1	Commander US Army Foreign Science and Technology Center ATTN: Research & Data Branch 220 7th Street, NE Charlottesville, VA 22901
1	Director US Army TRAC - Ft. Lee ATTN: ATRC-L, R. Cameron Fort Lee, VA 23801-6140
3	Commander US Army Materials Technology Laboratory ATTN: AMXMR-ATL SLCMT-MEC, W. Haskell SLCMT-MRD-S, K. Ofstedahl Watertown, MA 02172-0001
2	Commander US Army Strategic Defense Command ATTN: CSSD-H-MPL, Tech Lib CSSD-H-XM, Dr. Davies PO Box 1500 Huntsville, AL 35807

No. of Copies	Organization
2	Commander US Army Natick Research and Development Center ATTN: AMDNA-D, Dr. D. Sieling STRNC-UE, J. Calligeros Natick, MA 01762
1	Commander US Army Engineer Division ATTN: HNDED-FD PO Box 1500 Huntsville, AL 35807
3	Commander US Army Corps of Engineers Waterways Experiment Station ATTN: CAWES-SS-R, J. Watt CAWES-SE-R, J. Ingram CAWES-TL, Tech Lib PO Box 631 Vicksburg, MS 39180-0631
1	Commander US Army Research Office ATTN: SLCRO-D PO Box 12211 Research Triangle Park, NC 27709-2211
3	Commander US Army Nuclear & Chemical Agency ATTN: ACTA-NAW MONA-WE Tech Lib 7500 Backlick Rd., Bldg. 2073 Springfield, VA 22150
1	Director HQ, TRAC RPD ATTN: ATRC-RPR, Mr. Radda Fort Monroe, VA 23651-5143
1	Director TRAC-WSMR ATTN: ATRC-WC, Mr. Kirby White Sands Missile Range, NM 88002-5502

No. of Copies Organization

1 Director
TRAC-FLVN
ATTN: ATRC
Fort Leavenworth, KS 66027-5200

1 Commander
US Army Test & Evaluation Command
Nuclear Effects Laboratory
ATTN: STEWS-TE-NO,
Dr. J. L. Meason
PO Box 477
White Sands Missile Range, NM 88002

2 Chief of Naval Operations
ATTN: OP-03EG
OP-985F
Department of the Navy
Washington, DC 20350

1 Director
Strategic Systems Projects Office
ATTN: NSP-43, Tech Library
Department of the Navy
Washington, DC 20360

1 Commander
Naval Electronic Systems Command
ATTN: PME 117-21A
Washington, DC 20360

1 Commander
Naval Facilities Engineering Command
ATTN: Technical Library
Washington, DC 20360

1 Commander
Naval Sea Systems Command
ATTN: Code SEA-62R
Department of the Navy
Washington, DC 20362-5101

1 Officer-in-Charge
Naval Construction Battalion Center
Civil Engineering Laboratory
ATTN: Tech Lib, Code L06C/L08A
Port Hueneme, CA 93041

No. of Copies Organization

1 Commanding Officer
Naval Civil Engineering Laboratory
ATTN: Code L51, J. Tancreto
Port Hueneme, CA 93043-5003

1 Commander
Naval Surface Warfare Center
ATTN: Code DX-21, Library
Dahlgren, VA 22448-5000

1 Commander (Code 533)
Naval Weapons Center
Tech Library
China Lake, CA 93555-6001

1 Commander
Naval Weapons Evaluation Fac
ATTN: Document Control
Kirtland AFB, NM 87117

1 Commander
Naval Research Laboratory
ATTN: Code 2027, Tech Library
Washington, DC 20375

1 Superintendent
Naval Postgraduate School
ATTN: Code 2124, Tech Library
Monterey, CA 93940

2 Air Force Armament Laboratory
ATTN: AFATL/DOIL
AFATL/DLYV
Eglin AFB, FL 32542-5000

1 AFESC/RDCS
ATTN: Paul Rosengren
Tyndall AFB, FL 32403

1 RADC (EMTLD/Docu Library)
Griffiss AFB, NY 13441

3 Air Force Weapons Laboratory
ATTN: NTE
NTED
NTES
Kirtland AFB, NM 87117-6008

No. of Copies	Organization
1	AFIT ATTN: Tech Lib, Bldg. 640/B Wright-Patterson AFB, OH 45433
1	FTD/NIIS Wright-Patterson AFB, OH 45433
1	US Department of Energy Idaho Operations Office ATTN: Spec Programs, J. Patton 785 DOE Place Idaho Falls, ID 83402
2	Director Idaho National Engineering Laboratory EG&G Idaho Inc. ATTN: Mr. R. Guenzler, MS-3505 Mr. R. Holman, MS-3510 PO Box 1625 Idaho Falls, ID 83415
1	Commander David Taylor Research Center ATTN: Code 522, Tech Info Ctr Bethesda, MD 20084-5000
1	Officer in Charge White Oak Warfare Center Detachment ATTN: Code E232, Tech Library 10901 New Hampshire Avenue Silver Spring, MD 20903-5000
1	Commanding Officer White Oak Warfare Center ATTN: Code WA501, NNPO Silver Spring, MD 20902-5000
1	Director Lawrence Livermore National Laboratory ATTN: Tech Info Dept L-3 PO Box 808 Livermore, CA 94550
1	Director NASA-Langley Research Center ATTN: Tech Lib Hampton, VA 23665

No. of Copies	Organization
4	Director Los Alamos National Laboratory ATTN: Mr. Th. Dowler, MS-F602 Dr. J. Chapyak, MS-F664 Doc Control for Reports Library PO Box 1663 Los Alamos, NM 87545
3	Director Sandia National Laboratories ATTN: Doc Control 3141 Mr. C. Cameron, Div 6215 Mr. A. Chabai, Div 7112 PO Box 5800 Albuquerque, NM 87185-5800
1	Director Sandia National Laboratories Livermore Laboratory ATTN: Doc Control for Tech Library PO Box 969 Livermore, CA 94550
1	Director National Aeronautics and Space Administration ATTN: Scientific & Tech Info Fac PO Box 8757, BWI Airport Baltimore, MD 21240
1	Director NASA-Ames Research Center Applied Computational Aerodynamics Branch ATTN: Dr. T. Holtz, MS 202-14 Moffett Field, CA 94035
2	Applied Research Associates, Inc. ATTN: N. H. Ethridge J. Keefer PO Box 548 Aberdeen, MD 21001
1	Aerospace Corporation ATTN: Tech Info Services PO Box 92957 Los Angeles, CA 90009

No. of Copies	Organization
1	Agbabian Associates ATTN: M. Agbabian 250 North Nash Street El Segundo, CA 90245
1	Applied Research Associates, Inc. ATTN: R. L. Guice 7114 West Jefferson Ave., Suite 305 Lakewood, CO 80235
1	Black & Veatch, Engineers-Architects ATTN: H. D. Laverentz 1500 Meadow Lake Parkway Kansas City, MO 64114
1	The Boeing Company ATTN: Aerospace Library PO Box 3707 Seattle, WA 98124
1	California Research & Technology, Inc. ATTN: M. Rosenblatt 20943 Devonshire Street Chatsworth, CA 91311
1	Carpenter Research Corporation ATTN: H. Jerry Carpenter 27520 Hawthorne Blvd., Suite 263 PO Box 2490 Rolling Hills Estates, CA 90274
1	Dynamics Technology, Inc. ATTN: D. T. Hove 21311 Hawthorne Blvd., Suite 300 Torrance, CA 90503
1	EATON Corporation Defense Valve & Actuator Div. ATTN: Mr. J. Wada 2338 Alaska Ave. El Segundo, CA 90245-4896
2	FMC Corporation Advanced Systems Center ATTN: Mr. J. Drotleff Ms. C. Krebs, MDP95 2890 De La Cruz Blvd. Box 58123 Santa Clara, CA 95052

No. of Copies	Organization
1	Goodyear Aerospace Corporation ATTN: R. M. Brown, Bldg. 1 Shelter Engineering Litchfield Park, AZ 85340
4	Kaman AviDyne ATTN: Dr. R. Ruetenik (2 cys) Mr. S. Criscione Mr. R. Milligan 83 Second Avenue Northwest Industrial Park Burlington, MA 01803
3	Kaman Sciences Corporation ATTN: Library P. A. Ellis F. H. Shelton 1500 Garden of the Gods Road Colorado Springs, CO 80907
1	Kaman Sciences Corporation ATTN: Mr. F. W. Balicki 6400 Uptown Boulevard N.E., Suite 300 Albuquerque, NM 87110
2	Kaman-TEMPO ATTN: DASIAC Don Sachs PO Drawer QQ 816 State Street Santa Barbara, CA 93102
1	Ktech Corporation ATTN: Dr. E. Gaffney 901 Pennsylvania Avenue, N.E. Albuquerque, NM 87111
1	Lockheed Missiles & Space Co. ATTN: J. J. Murphy Dept. 81-11, Bldg. 154 PO Box 504 Sunnyvale, CA 94086
2	McDonnell Douglas Astronautics Corporation ATTN: Robert W. Halprin K.A. Heinly 5301 Bolsa Avenue Huntington Beach, CA 92647

No. of Copies	Organization
1	Orlando Technology, Inc. ATTN: Mr. D. Matuska PO Box 855 Shalimar, FL 32579
2	Physics International Corporation 2700 Merced Street San Leandro, CA 94577
2	R&D Associates ATTN: Technical Library Dr. Allan Kuhl PO Box 9695 Marina Del Rey, CA 90291
1	R&D Associates ATTN: G. P.Ganong PO Box 9377 Albuquerque, NM 87119
2	Science Applications, Inc. ATTN: W. Layson John Cockayne PO Box 1303 1710 Goodridge Drive McLean, VA 22102
1	Science Applications International Corp. ATTN: Mr. J. Guest 2301 Yale Blvd. SE, Suite E Albuquerque, NM 87106
1	Sparta, Inc. Los Angeles Operations ATTN: I. B. Osofsky 3440 Carson Street Torrance, CA 90503
1	Sunburst Recovery, Inc. ATTN: Dr. C. Young PO Box 2129 Steamboat Springs, CO 80477
1	Sverdrup Technology, Inc. ATTN: R. F. Starr PO Box 884 Tullahoma, TN 37388

No. of Copies	Organization
3	SRI International ATTN: Dr. G. R. Abrahamson Dr. J. Gran Dr. B. Holmes 333 Ravenswood Avenue Menlo Park, CA 94025
2	S-CUBED A Division of Maxwell Laboratories, Inc. ATTN: C. E. Needham Dr. Lynn Kennedy 2501 Yale Blvd., SE Albuquerque, NM 87106
3	S-CUBED A Division of Maxwell Laboratories, Inc. ATTN: Technical Library R. Duff K. Pyatt PO Box 1620 La Jolla, CA 92037-1620
1	Texas Engineering Experiment Station ATTN: Dr. D. Anderson 301 Engineering Research Center College Station, TX 77843
1	Thermal Science, Inc. ATTN: R. Feldman 2200 Cassens Dr. St. Louis, MO 63026
1	TRW Ballistic Missile Division ATTN: H. Korman, Mail Station 526/614 PO Box 1310 San Bernadino, CA 92402
1	Battelle ATTN: TACTEC Library, J. N. Higgins 505 King Avenue Columbus, OH 43201-2693

No. of
Copies Organization

1 California Institute of Technology
ATTN: T. J. Ahrens
1201 E. California Blvd.
Pasadena, Ca 91109

2 Denver Research Institute
ATTN: Mr. J. Wisotski
Technical Library
PO Box 10758
Denver, CO 80210

1 Massachusetts Institute of Technology
Aeroelastic and Structures Research Laboratory
ATTN: Dr. E. A. Witmer
Cambridge, MA 02139

1 Massachusetts Institute of Technology
ATTN: Technical Library
Cambridge, MA 02139

2 New Mexico Engineering Research Institute (CERF)
University of New Mexico
ATTN: Dr. J. Leigh
Dr. R. Newell
PO Box 25
Albuquerque, NM 87131

1 Northrop University
ATTN: Dr. F. B. Safford
5800 W. Arbor Vitae St.
Los Angeles, CA 90045

4 Southwest Research Institute
ATTN: Dr. W. E. Baker
A. B. Wenzel
Dr. C. Anderson
S. Mullin
6220 Culebra Road
San Antonio, TX 78284

1 Stanford University
ATTN: Dr. D. Bershader
Durand Laboratory
Stanford, CA 94305

No. of
Copies Organization

3 University of Maryland
Department of Mechanical Engineering
ATTN: Dr. W. Fourney
Dr. R. Dick
Dr. J. Williams
College Park, MD 20742

Aberdeen Proving Ground

1 Cdr, USATECOM
ATTN: AMSTE-TE-F, L. Teletski

1 Cdr, USATHMA
ATTN: AMXTH-TE

USER EVALUATION SHEET/CHANGE OF ADDRESS

This laboratory undertakes a continuing effort to improve the quality of the reports it publishes. Your comments/answers below will aid us in our efforts.

1. Does this report satisfy a need? (Comment on purpose, related project, or other area of interest for which the report will be used.) _____

2. How, specifically, is the report being used? (Information source, design data, procedure, source of ideas, etc.) _____

3. Has the information in this report led to any quantitative savings as far as man-hours or dollars saved, operating costs avoided, or efficiencies achieved, etc? If so, please elaborate. _____

4. General Comments. What do you think should be changed to improve future reports? (Indicate changes to organization, technical content, format, etc.) _____

BRL Report Number BRL-TR-3213 Division Symbol _____

Check here if desire to be removed from distribution list. ____

Check here for address change. ____

Current address: Organization _____
Address _____
_____

DEPARTMENT OF THE ARMY

OFFICIAL BUSINESS

BUSINESS REPLY MAIL
FIRST CLASS PERMIT No 0001, APG, MD

Postage will be paid by addressee.

NO POSTAGE NECESSARY IF MAILED IN THE UNITED STATES